QUANTITATIVE AGE-AT-DEATH ESTIMATION: A THREE-DIMENSIONAL MORPHOLOGICAL ANALYSIS OF THE STERNAL EXTREMITY OF THE RIB

by

Audrey D. Schaefer, BA

A thesis submitted to the Graduate Council of
Texas State University in partial fulfillment
of the requirements for the degree of
Master of Arts
with a Major in Anthropology
December 2017

Committee Members:

Nicholas P. Herrmann, Chair

Daniel J. Wescott

Deborah Cunningham

FAIR USE AND AUTHOR'S PERMISSION STATEMENT

Fair Use

Duplication Permission

DEDICATION

To Audrey and John Bagliani (Aka: Grammy and PopPop),

for instilling in me the value of hard work and education.

ACKNOWLEDGEMENTS

I would like to acknowledge Dr. Herrmann for all his support and guidance throughout this process and for providing me with an abundance of opportunities to grow within this field. I would also like to thank my committee, Dr. Wescott and Dr. Cunningham, for your support and all the lessons you have taught me during my graduate career. Additionally, thank you to Dr. Cunningham and Devora Gleiber for taking time to teach me how to use the North Star x5000 microCT system. Your patience and willingness to help was so appreciated.

I extend a sincere thank you to Dr. Steadman for allowing me to visit University of Tennessee and borrow ribs for my research. To Detelina Stoyanova, you graciously dedicated time to generate a custom version of *forAge* for my thesis. Thank you, I hope to return the favor someday. Also, thank you to Dr. Franklin Damann for opening my eyes to the world of 3D imaging/modeling. It has set me on an amazing path of discovery within this field.

To my Mom, Mary, and Eugene, you each taught me to have courage, perseverance, and confidence in all I do. These values have gotten me to this point and I would not be able to continue to follow my dreams without your unwavering support. To my Cohort, thank you for the constant support, whether it was through dinners, happy hours, or late study nights, I could not have imagined this journey with anyone else. To the cohorts above and below mine, thank you for setting an amazing precedent to succeed. You all inspire and motivate me every day.

TABLE OF CONTENTS

LIST OF TABLES

Table **Page**

LIST OF FIGURES

Figure **Page**

LIST OF ABBREVIATIONS

Abbreviation	Description
BE	Bending Energy
CT	Computed Tomography
FACTS	Forensic Anthropology Center at Texas State
GEFARL	Grady Early Forensic Anthropology Research Laboratory
PCA	Principal Component Analysis
PC	Principal Component
PLY	Polygon File Format
RMSE	Root Mean Squared Error
SAH	Slice-Algee-Hewitt Score
TIFF	Tag Image File Format
TPS	Thin Plate Splines
VC	Ventral Curvature
3D	3-Dimensional

I. INTRODUCTION

Age-at-death estimation is a critical step in construction of the biological profile. Over the years, many aspects of the skeleton have been used to assess age-at-death. Some of the most utilized age-at-death indicators for skeletally mature individuals include the pubic symphysis, auricular surface, and the sternal rib end. The methodologies developed using these skeletal indicators are reliant on age-based phase categorization made from subjective macroscopic assessment of the skeletal indicator's morphology (Todd 1920, İşcan and Loth 1984, Lovejoy et al. 1985, Brooks and Suchey 1990, Buckberry and Chamberlain 2002, Hartnett 2010b). Although these methodologies are relatively simple and accessible, phase-based techniques have been criticized for their lack of objectivity and high rate of error (Slice and Algee-Hewitt 2015).

Recently, the field of forensic anthropology has moved to increase standardization and reduce subjectivity in the "less rigorous observational methodologies" (Christensen 2009:1216). This re-assessment of methodologies has increased due to Supreme Court cases, such as Daubert v. Merrell Dow Pharmaceuticals, Inc., General Electric Co. v. Joiner, and Kumho Tire Co. v. Carmichael (Christensen 2009). These cases called the "reliability and relevance of scientific testimony" into question, thus placing pressure on disciplines lacking standardization and statistically sound objective methodologies (Christensen 2009:1212). These decisions have dictated a need for improved,

standardized methods, and quantified results in the field of forensic anthropology (Slice and Algee-Hewitt 2015).

Three recent studies sought to address these methodological issues using the "most reliable" and the most widely used skeletal indicator of age-at-death: the Suchey-Brooks pubic symphysis phase method (Slice and Algee-Hewitt 2015:836, Stoyanova et al. 2015, Stoyanova et al. 2017). These studies together generated a fully objective method of age-at-death estimation by quantifying the surface morphology of the pubic symphysis. The authors collected point cloud data from laser surface scans and generated three different shape scores to quantify the surface topography (Slice and Algee-Hewitt 2015, Stoyanova et al. 2015, 2017). They generated a program, *forAge*, to read point cloud files and automatically calculate the shape scores and corresponding estimated age-at-death for the pubic symphysis. These methodologies produced similar age estimation results compared to the original Suchey-Brooks phase-based methodology, but this new method of age estimation was performed in an objective and quantitative manner. If this method of quantitative age-at-death estimation demonstrated production of an accurate age-at-death assessment that meets the Daubert standards, perhaps a quantitative and objective methodology would also prove accurate and reliable for other age-at-death indicators such as the sternal end of the rib.

Research Questions

This thesis will examine quantitative methodologies using the sternal end of the rib as an age-at-death indicator. The research will seek to answer two questions: Can the morphology of the sternal extremity of the rib be quantitatively measured to generate an objective age-at-death estimate? Will this method provide a more accurate age-at-death assessment than the original İşcan-Loth Rib Age Determination (1984a) phase method? This study will quantitatively assess the morphology of the sternal extremity of the rib through collection of 3D point cloud data via microCT imaging. Morphological shape scores will be generated using the *forAge* program. These shape scores, which quantify the surface morphology of the sternal rib end, will be used to estimate age-at-death.

II. LITERATURE REVIEW

Age-at-death Estimation

Skeletal age-at-death estimation must take both chronological and biological age into consideration. Chronological age is aligned with time; it is the age that we are associated with during life. Biological age, also called physiological age, refers to the changes that occur in the skeleton based on time and life experiences (Christensen et al. 2014, Uhl 2013, Slice and Algee-Hewitt 2015). Chronological age and biological age are correlated; however, this correlation is not uniformly useful because biological age varies widely between two individuals. Variable degenerative changes throughout life allow for a disjunction between chronological age and biological age in the skeleton. Thus, adult age-at-death estimation is often more difficult to assess because it is correlated with degenerative skeletal changes (Christensen et al. 2014). Adult age-at-death is assessed both morphologically and histologically. This thesis focuses on morphological methodologies.

Adult Age-at-death Indicators

Traditional adult age-at-death analyses have revolved around several skeletal indicators including the morphology of the major joints (e.g., pubic symphysis, auricular surface, sternal rib end), cranial sutures, dental morphology, and bone histology. The methodologies based on joint indicators are similar and have experienced revisions since

originally developed. The original joint-based methods generalized and simplified the varied temporal changes in morphology of the indicator through generation of phases that represent the observed age-related morphological changes. To perform these phase-based methodologies, the observer examines the morphology of the skeletal indicator and chooses what they think is the most appropriate phase description that closely aligns with the observed morphology of the skeletal joint indicator (Todd 1920, İşcan and Loth 1984, Lovejoy et al. 1985, Brooks and Suchey 1990, Buckberry and Chamberlain 2002).

Baccino et al. (1999) evaluated phase-based methods including the pubic symphysis phase analysis method and the İşcan-Loth Rib Age Determination method, among others. Although restricted to a small sample size, Baccino et al. (1999) found that combined methods of age assessment, rather than use of a single indicator, provided a more accurate age-at-death estimation. A more recent study by Matrille et al. (2007) performed similar research analyzing the Lamendin dental method, the pubic symphysis, auricular surface, and the sternal end of the rib. Contrary to Baccino et al. (1999), Matrille et al. (2007) found that a combination of aging methodologies did not provide higher accuracy in age estimation as compared to use of a singular method.

More recently, a software was developed to implement idea supported by Baccino et al. (1999) that examination of more than one skeletal age indicator may provide a more accurate picture of the true age-at-death. The program, ADBOU, combined several age-at-death methods from skeletal indicators such as cranial sutures, the pubic symphysis, and the auricular surface (http://math.mercyhurst.edu/~sousley/Software/). ADBOU

employed updated scoring procedures and new statistical analyses for traditional phase-based indicators with the goal of obtaining age-at-death estimation with statistically sound error estimates (Boldsen et al. 2002). Although the program still required input of scores from phased-based categorization, ADBOU incorporated the statistical method of transition analysis, which helped generate age-at-death estimates with known error and statistical confidence intervals (Boldsen et al. 2002).

Over time, the phase-based methods have been examined for accuracy and performance often leading to adjustments such as expand sample sizes and modified phase descriptions (Brooks and Suchey 1990, Buckberry and Chamberlain 2002, Hartnett 2010a, Hartnett 2010b). For some, advanced statistics allowing for calculation of confidence intervals were added to generate a more statistically robust association of the skeletal indicator's morphology to age-at-death. But these adjustments to the traditional methods are still driven by phase-based categorization from subjective macroscopic analysis of the surface morphology. This study aims to move away from traditional phase-based categorization and towards quantification of the surface morphology itself.

The Rib as an Age-at-Death Indicator

The İşcan-Loth Rib Age Determination method is widely used today to estimate the age-at-death of unknown individuals (Garvin and Passalaqua 2012). İşcan and Loth (1984a) generated an age-at-death estimation technique based on the morphological changes in the sternal end of the right fourth rib in white males. The authors examined

features such as pit depth, pit shape, rim morphology surrounding the pit, and overall bone structure. A nine-phase (0 to 8) system based on age-related morphological changes was generated (Appendix A). Each phase was accompanied by a description and photos for comparison (İşcan and Loth 1984a). The authors found that the mean age associated with a single rib increased as the allotted phase increased (İşcan and Loth 1984a). The greatest observed morphological changes occurred in the first four phases, corresponding to the early stages of formation in younger individuals (İşcan and Loth 1984a). The age ranges allotted for later phases were much wider due to increased variability in rib morphology. The authors later supplemented their original method to account for morphological differences between males and females and between populations (İşcan and Loth 1985, 1987).

The İşcan-Loth Rib Age Determination method has been criticized on several counts: high rates of inter- and intra-observer error, population specificity of the method, large age ranges associated with each phase, and weak statistical methodologies (Hartnett 2010b, İşcan and Loth 1984a). İşcan and Loth (1984a) discussed the implications of factors influencing rib morphology such as disease, occupation, and trauma. These factors all affect the accuracy of morphologically assessed age-at-death estimation (İşcan and Loth 1984a). Additionally, use of the rib as an age-at-death indicator, as compared to other joint indicators, raises some issues. For example, those who attempt to estimate the age-at-death of archaeological remains using the rib as an indicator often note the poor preservation of the rib and issues with recovery of ribs such as increased risk of post

mortem damage (Russell 1993, Dedouit 2008). When rib specimens are obtained as autopsy samples, time-consuming bone preparation is necessary, delaying analysis of the specimen (Dedouit 2008).

Numerous studies critically evaluated the İşcan-Loth Rib Age Determination technique, resulting in conflicting conclusions. Russell et al. (1993) examined the accuracy of the İşcan-Loth Rib Age Determination method. The results were consistent with the general tendency to underage the individual while using this method, which was found to be more severe in the black male population (Russell et al. 1993). The authors also discussed the ambiguity in assessment of bone quality and density of the rib which negatively influenced accurate age assessment (Russell et al. 1993).

Baccino et al. (1999) found when the İşcan-Loth Rib Age Determination method was compared to other aging methods, it was only moderately accurate in estimating age-at-death, relative to other skeletal indicators. Matrille (2007) found that when divided into three broad age groups (young, middle-aged, and old), the İşcan-Loth Rib Age Determination method was the least accurate for the young age groups and most accurate for the old age groups. This finding was contradicted by Salem et al. (2014), who found that young phases, below phase 5, more accurately estimated the actual age of the individual.

Hartnett (2010a, 2010b) examined both the pubic symphysis and the sternal rib end as age indicators. She suggested that the rib might be a better age-at-death indicator than the pubic symphysis due to its comparatively lower rates of inter-observer and intra-

observer error. However, the İşcan-Loth Rib Age Determination method was not highly accurate. Hartnett's (2010b) study suggested revision of the İşcan-Loth Rib Age Determination method and provided modified phase descriptions (Appendix B). Hartnett (2010b) suggested increased emphasis be placed on the bone quality and density, weight, and texture of the rib in the phase descriptions. Hartnett's (2010b) improved phase descriptions and age ranges were tested by Merritt (2014), who found that Hartnett's (2010b) modifications provided only slightly more accurate age-at-death estimation as compared to the original İşcan-Loth method.

Fanton et al. (2010) sought to provide an objective, statistical review of the rib as an age-at-death indicator. Pit depth, pit shape, and rim configuration proved to be poor morphological predictors of age due to various shortcomings of the İşcan-Loth Rib Age Determination method (Fanton et al. 2010). The pit depth indicator was found to have minimal association with age-at-death as compared to the other indicators (Fanton et al. 2010). Fanton et al. (2010) recommended improvement of the İşcan-Loth Rib Age Determination method to allow for more detailed phase descriptions, utilization of modern imaging tools, and employment of multivariate statistics (Fanton et al. 2010).

Three additional studies examined the İşcan-Loth Rib Age Determination method on different populations. For Tunisian, Turkish, and Indian known-age samples, the American white method provided accurate age-at-death estimations (Yavuz et al. 1998, Salem 2014, Meena and Rani 2014). However, the İşcan-Loth method did not generate accurate age-at-death assessments for South African Blacks and Spanish known-age

samples (Oettle et al. 2000, MacAluso and Lucena 2012). Martrille et al. (2007) and Russell et al. (1993) did not find a significant difference between age estimation for American blacks and whites, which contradicts İşcan and Loth's (1987) findings.

An alternative method to the phase-based methods for age-at-death estimation was suggested by İşcan in 1984 (Meena and Rani 2014). This method was component-based, where the morphology of the rib end was divided into three separate components: pit depth, pit shape, and rim and wall configuration (İşcan 1984b, Verzeletti 2010). In this component-based method, each component was assessed separately then was assigned to its own series of phases. Several researchers reevaluated the component-based method from the rib and its accuracy in age-at-death estimation as compared to the original phase-based method (Verzeletti 2010, MacAluso and Lucena 2012, Meena and Rani 2014). Verzeletti (2010) tested the method on Italian males and subsequently adjusted the original İşcan (1984b) component method to include expanded age classes for each component. MacAluso and Lucena (2012) tested this component method on a Spanish sample and found a higher amount of error in age estimation. Meena and Rani (2014) tested Verzeletti's (2010) method on an Indian sample and found that pit depth was the poorest indicator of age as compared to pit shape and rim and wall configuration.

The rib as an age-at-death indicator does show promise even if the literature suggests contradictory findings. The rib exhibits age-related changes throughout life. Although evidence of population differences in the rib is dependent on the population under study, the research discussed above suggests that the use of the rib for age

estimation is applicable to multiple populations. The İşcan-Loth Rib Age Determination method also displayed a common observation of all skeletal aging methodologies, the overestimation of younger individuals and the underestimation of older individuals (Russell et al. 1993, Matrille et al. 2007, MacAluso and Lucena 2012, Salem et al. 2014). Additionally, the İşcan-Loth Rib Age Determination method shows little inter- and intra-observer error as compared to other phase-based methods (Hartnett 2010b, Meena and Rani 2014). It is possible that this observer error can be further reduced with quantification and objectification of the method as a whole. It is time to investigate alternative methods of morphological analysis to phase-based and component-based analyses.

Two studies attempted an alternative method of bone acquisition for use in age-at-death estimation. Dedouit et al. (2008) and Moskovitch et al. (2010) generated 3D renditions of the sternal end of the first and fourth rib and compared phase-based assessment between the 3D model and the bone itself. Both researchers cited no difference between phase assessment of the real ribs and the 3D models. The criticisms of using the rib for age-at-death analysis addressed above may be avoided with use of non-invasive, objective computed tomography (CT) or 3-dimensional (3D) scanning methodologies. These 3D methodologies remove the need for bone removal and preparation and potentially expand the application of age-at-death methodologies to living individuals (Dedouit et al. 2008, Dedouit et al. 2014). Dedouit et al. (2008) even suggested the increased ease of acquisition and improved image quality of CT technology

over the past several years, indicating the promise of this technology in forensic anthropological methodologies.

Morphological Quantification

Three recent studies sought to generate a means of quantitative age-at-death estimation using geometric morphometric shape analysis. The first study by Slice and Algee-Hewitt (2015) used raw x, y, z point cloud data extracted from laser scans of pubic symphyses to generate a fully quantitative method of age estimation. The authors generated a known age sample of right and left pubic symphyses from males and females of varied ancestries (Slice and Algee-Hewitt 2015). The authors applied a methodology based on a variance score calculated from the point cloud data representing the symphyseal surface morphology. First, principal component analysis (PCA) was applied to the point cloud data. This PCA generated three principal component (PC) values based on the three x, y, and z coordinates in the point cloud data. These PC values aimed to represent the spatial variance and morphological variation encompassed within the morphology of the pubic symphysis (Slice and Algee-Hewitt 2015). The third PC value, which represented the variance in z-coordinate, was used to generate what the authors call the Slice-Algee-Hewitt (SAH) shape score. Age-at-death was then estimated in a linear regression model using the SAH value and known age-at-death (Slice and Algee-Hewitt 2015).

The second study expanded on Slice and Algee-Hewitt's (2015) research by applying a different methodology to quantify the shape of the pubic symphysis. As compared to Slice and Algee-Hewitt's (2015), Stoyanova and colleagues (2015) adjusted the sample to only include males of white ancestry. The new type of surface morphology quantification proposed by Stoyanova et al. (2015) measured the pubic symphysis using Thin Plate Spline (TPS) analysis. For accurate application of TPS analysis, each model must be positioned in the same plane and orientation. Therefore, prior to TPS analysis, a PCA analysis was performed to automatically orient each pubic symphysis (Stoyanova et al. 2017). Then, the TPS analysis generated a hypothetical thin metal plate that bends across the surface in question (Stoyanova et al. 2015). As the plate bends, the minimum amount of bending energy (BE) used to match the plate to the surface morphology is calculated. Thus, this method of surface quantification generated the BE shape score. The authors used the minimum bending energy (BE) shape score in linear regression analysis to estimate age-at-death (Stoyanova et al. 2015).

Lastly, a third study expanded the sample sizes, added a third morphological shape score, adjusted formulae, and included multivariate regression analysis (Stoyanova et al. 2017). The third shape score analyzed the ventral curvature of the pubic symphysis and cannot be applied to other skeletal indicators.

All three studies produced methodologies that output similar age-at-death estimation results compared to the original Suchey-Brooks phase-based methodology (Stoyanova et al. 2017). The third study even produced improved age-at-death

estimations compared to the Suchey-Brooks phase-based methodology. In summary, these authors generated a novel quantified and objective method that proved to work well in providing accurate age-at-death estimations for the pubic symphysis (Slice and Algee-Hewitt 2015, Stoyanova et al. 2015).

This Study

This research applies the methodology of quantitative age-at-death estimation developed by Slice, Algee-Hewitt, Stoyanova and colleagues to the sternal end of the rib. Expansion of this quantitative age-at-death estimation methodology will help to further investigate alternative forms of age-at-death estimation that remove traditional subjective phase-based assessment. The field of forensic anthropology will benefit from the continuing effort to remove subjectivity and quantify methodologies.

This research will generate microCT scans of a fully representative sample of age-based morphological changes in sternal rib ends. The point cloud data from the CT scans will be imported into the *forAge* program from which SAH and BE shape scores will be extracted. These shape scores will quantitatively represent the morphology of the sternal end of the rib and will be used in subsequent regression analysis to perform an age-at-death estimation.

III. MATERIALS AND METHODS

Materials

Sample. The sample consists of a total of 80 human sternal rib end surface models. These 80 surface models aim to represent the range of age-related morphological changes in the sternal rib end. Selection of ribs was based on a sampling system that was divided into five-year age increments (e.g., ages 20-24) ranging from 15-95 years (Figure 1). Each age increment contains three female and three male ribs. This sample was assembled from both the Texas State Donated Skeletal Collection (n=49) and the University of Tennessee W. M. Bass Skeletal Collection (n=31) (Table 1). Both collections consist of modern, donated skeletal material, therefore age-at-death, sex, and reported ancestry are known. Due to sampling issues, collection of six ribs per age increment was unobtainable. This sample lacks females under the age of 34. Additionally, there is only one female and two males for the 90-94 age increment. The sample ranges in age from 16 to 93 years with an average age of 59 years. This sample was supplemented with an additional 41 rib surfaces, which consist of the İşcan-Loth Rib Age Determination casts.

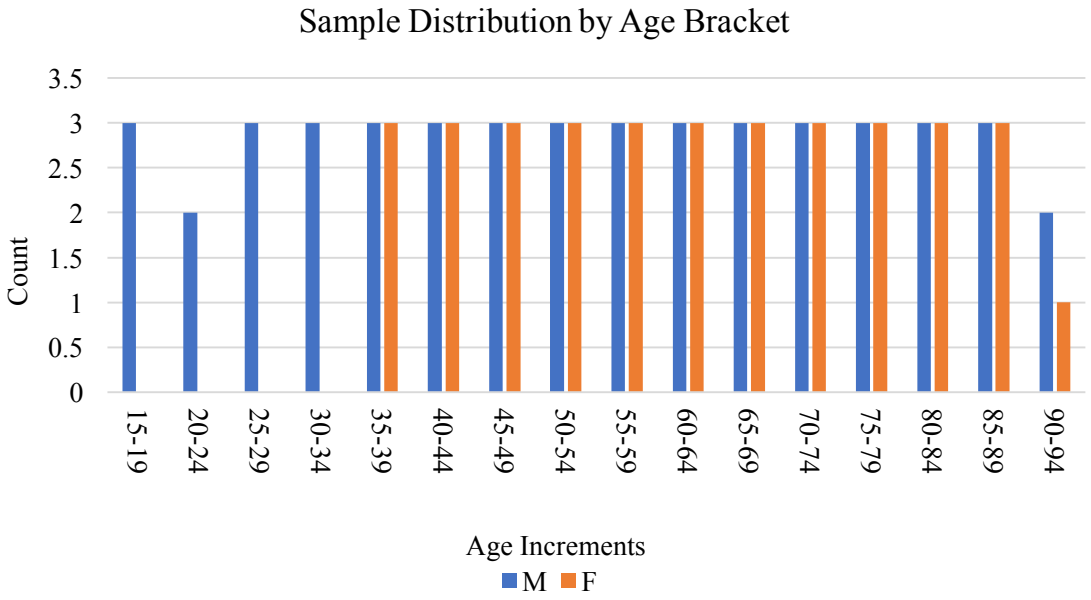

Figure 1. Sample distribution of males and females by age brackets.

Table 1. Origin of sample

Location of Origin	Count
Texas State University	49
University of Tennessee, Knoxville	31
İşcan-Loth Rib Age Determination casts	41
Total	121

Sample parameters, including sex and rib number, were selected based on the samples from İşcan and Loth (1984a), Slice and Algee-Hewitt (2015), and Stoyanova et al. (2015). This sample included both males and females (Table 2). The right rib was given priority, however left ribs were substituted when the right side was damaged or absent. Additionally, this sample included ribs from individuals of self-reported white

ancestry for several reasons: to obtain a larger sample size, to maintain consistency with the Stoyanova et al. (2015) study on the pubic symphysis, and to remove the issue of ambiguity in use of the İşcan-Loth Rib Age Determination method between different populations.

Table 2. Sample counts by sex and casts.

Sex	Count	
	Without Casts	With Casts
Males	47	68
Females	33	53
Total	80	121

Due to the indistinct nature of rib sequence morphology, it is often difficult to accurately assess rib number. İşcan and Loth (1984a:1095) used the fourth rib for analysis because "it can be easily obtained." Thus, the fourth rib was given priority in this study. However, various authors suggested the possibility of little or no significant difference in the sternal morphologies of ribs three and five as compared to rib four (Ozgur et al 2004, Nikita 2013). Therefore, when the fourth rib was missing or exhibited post-mortem damage or pathological conditions, the fifth rib was used. Selection of ribs began with sequencing of the ribs in anatomical order in accordance with Mann (1993). The sequencing method consisted of placing a set of ribs on a table with the inferior side facing up. The curvature of the body along with the shape and size of the rib was taken in consideration as each rib was placed in its anatomical position (Mann 1993). Once all 12

ribs were aligned, the correct rib was selected. Rib priority was chosen in the following order: right fourth, left fourth, right fifth, and lastly, left fifth (Table 3).

Table 3. Sample counts by side and rib number

Side	Rib Number	Count	Total
Right	Fourth	64	67
	Fifth	3	
Left	Fourth	11	13
	Fifth	2	
Total			80

Table 4. Sample counts by rib number

Rib #	Count
Fourth Rib	75
Fifth Rib	5
Total	80

Materials. The materials required for this research include: North Star x5000 microCT system and accompanying software, İşcan-Loth Rib Age Determination casts, 3D modeling software, the *forAge* program, Microsoft Excel, and R-statistical environment. The North Star x5000 microCT scanner and the accompanying software, efxDR and efxCT are housed in the Grady Early Forensic Anthropology Laboratory (GEFARL) at Texas State University. This software was necessary to obtain CT scans and reconstruct 3-dimensional images. The İşcan-Loth Rib Age Determination Casts

were available at GEFARL. Two forms of 3D modeling software, Avizo 9.4 and Meshlab v. 2016.12, were utilized for editing and exporting of final surface models. The *forAge* program allows for the import of point cloud data and subjects this data to three types of morphometric shape analysis. The program is free and is available for download at http://morphlab.sc.fsu.edu/software/forAge/. The final data used in this research was collected from a custom version of *forAge*, provided by Detelina Stoyanova. The custom *forAge* program, along with Microsoft Excel and R statistical environment, were used for morphological and statistical analyses (R Core Team 2016).

Methods

The methods for this research revolved around three steps: data collection, morphological analysis, and statistical analysis (Figure 2).

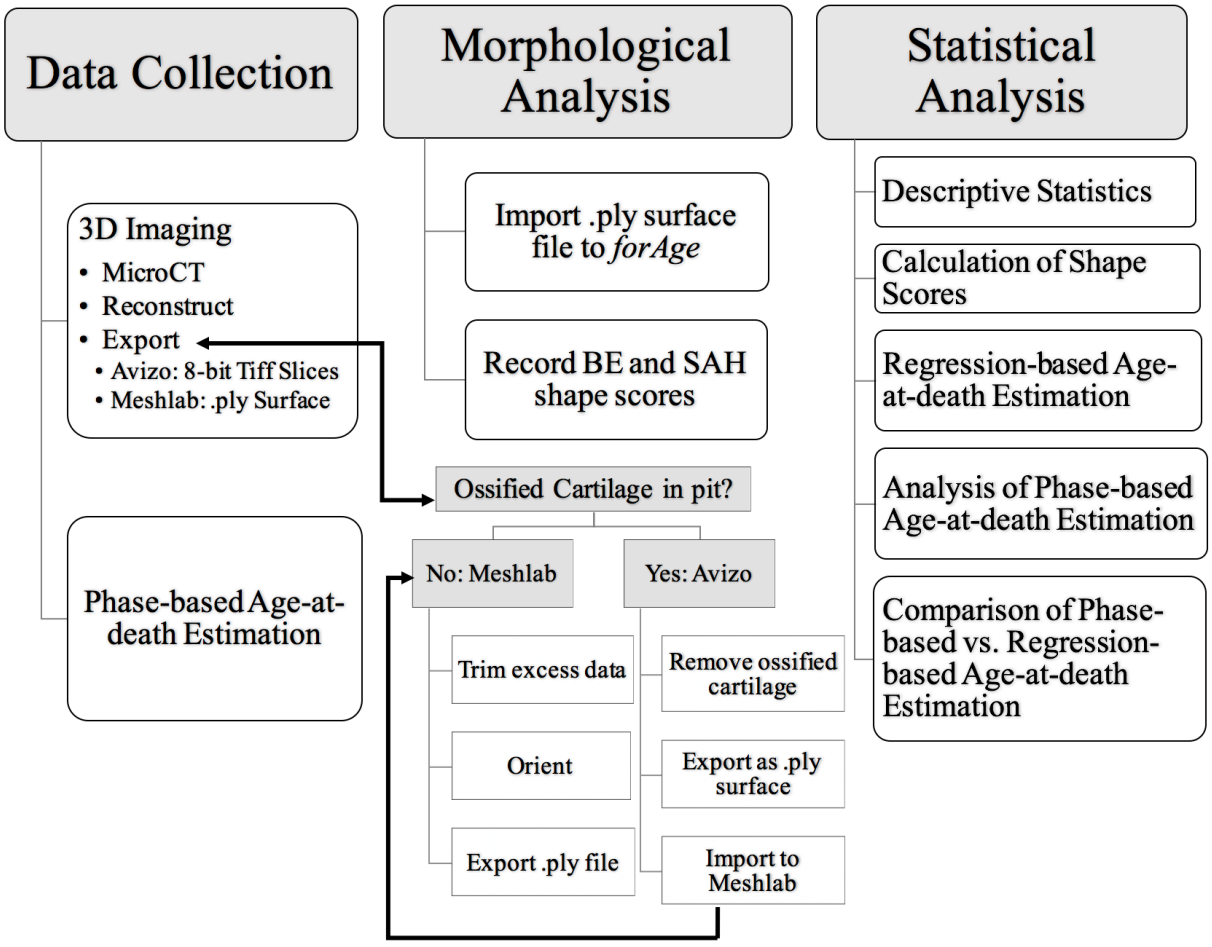

Figure 2. Diagram of methods

Data collection. The data collection methodology aimed to quantitatively assess the aspects of the sternal rib morphology, such as pit depth, pit shape, rim configuration, and bone quality, discussed by İşcan and Loth (1984a) using the morphological quantification methods presented by Slice and Algee-Hewitt (2015) and Stoyanova et al. (2015).

This study used a North Star x5000 microCT scanner to collect 3-dimensional images of each rib. Scan parameters included resolution and x-ray settings that impact the quality of a CT image. Tradeoffs in choosing these parameters include obtaining a detailed, high-resolution image in an acceptable amount of time, resulting in a reasonable file size. A total of twenty-seven scans were performed on sets of three ribs. Ribs were grouped based on uniformity of size and shape. A fixture to hold the rib for CT imaging was made from florist foam and elements were secured with excess foam before each scan (Figure 3). It was necessary that the fixture held the ribs completely motionless throughout the imaging process to avoid image blur. The scan parameters varied but generally had energy settings around ~100 kV and ~200 mA. Each scan was acquired at 1 frame per second and scan time was typically around 1 hour and 30 minutes. After scanning, the images were reconstructed in the efxCT software. Each set of 3 ribs was cropped and saved as individual files.

Figure 3. Three ribs secured in a green foam mount for microCT scanning.

Next, the ribs were separated into two groups: ribs with and without excess ossified cartilage in the pit of the sternal rib end. Ribs that lacked ossified cartilage in the pit were immediately exported after reconstruction as an Ascii Polygon File Format (ply) surface file for editing in Meshlab v. 2016.12. To obtain the BE and SAH shape scores from the *forAge* program, all ply surface files must only contain the surface morphology of the rib. The Meshlab v. 2016.12 editing process aimed to remove excess data, such as the trabeculae and the rib walls, to isolate solely the morphology of the surface of the sternal rib end (Figures 4 and 5). Ribs with ossified cartilage (n=12) were exported as 8-

bit TIFF slices for removal of the cartilage in Avizo 9.4. Once the ossified cartilage was removed, the edited rib model was exported as a ply surface file for additional editing in Meshlab v. 2016.12. In summary, all ribs were edited in Meshlab v. 2016.12 and only 12 ribs were edited in Avizo 9.4 prior to Meshlab v. 2016.12 editing (Figure 2).

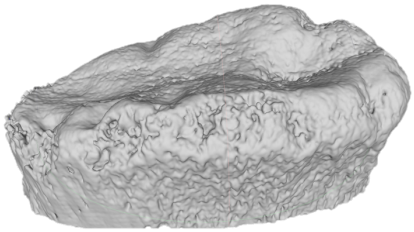

Figure 4. Surface model of the right, fourth rib from individual D19-2012 before removal of excess data in Meshlab v. 2016.12.

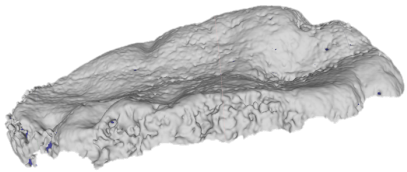

Figure 5. Surface model of the right, fourth rib from individual D19-2012 after removal of excess data in Meshlab v. 2016.12.

Lastly, to collect phase-based data for the sample of 80 ribs, each rib was scored using the İşcan-Loth (1984a, 1985) and Hartnett (2010b) phase-based age-at-death methods. The İşcan-Loth Rib Age Determination casts were not scored, but were used to aid in phase assessment. All ribs were separated by sex, then a student volunteer

randomized the ribs to provide for blind assessment by the author. The author scored each rib using the two phase-based methods at three separate times. This phase-based data was later used to compare the traditional phase-based methods and the new regression-based method generated by this research.

Morphological Analysis. Slice and Algee-Hewitt (2015) and Stoyanova et al. (2015) generated a free software titled *forAge* to calculate the raw SAH and BE shape scores and their respective age-at-death from surface scans of pubic symphyses. This study uses the *forAge* program to calculate the raw BE and SAH shape scores for each rib ply surface file (Figure 6). The age-at-death estimations and the third shape score (ventral curvature (VC)) automatically provided by the *forAge* program were ignored because they are specific to the pubic symphysis and are not applicable to the rib.

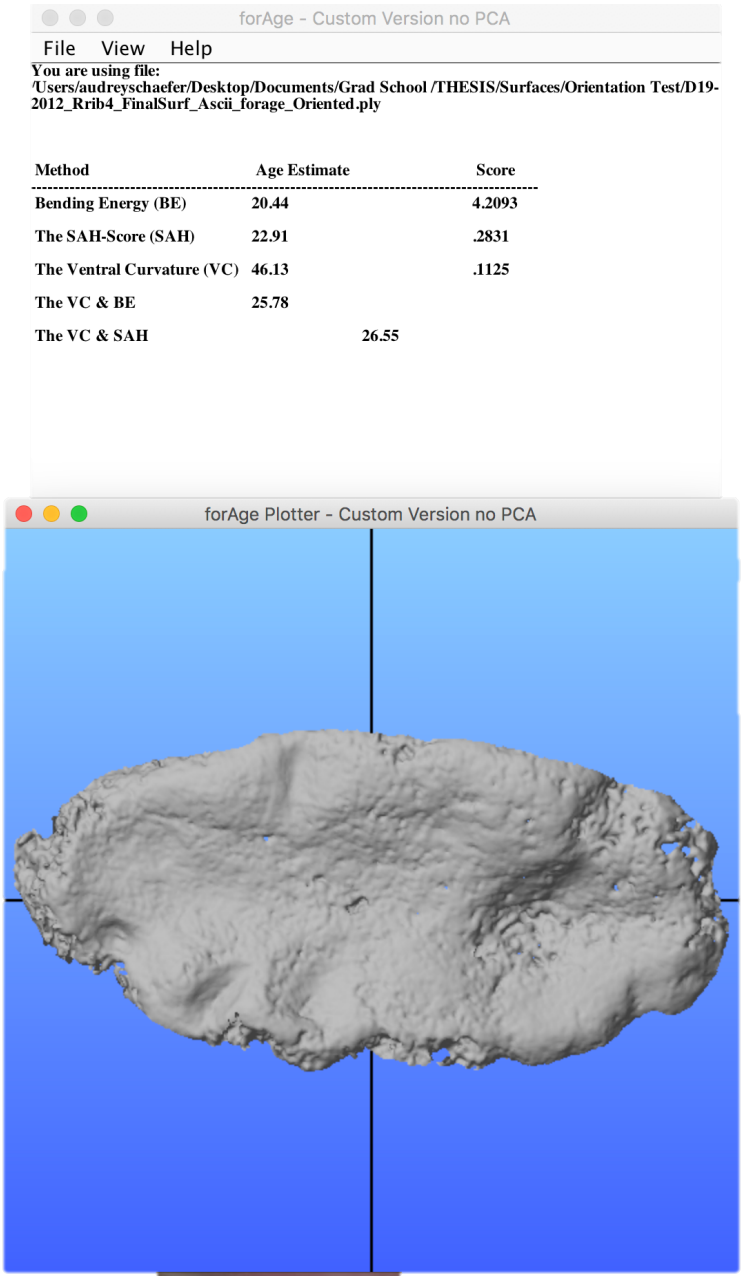

Figure 6. *forAge* output for the right, fourth rib from individual D19-2012.

Most of the rib surfaces were easily imported into the *forAge* program, but some surfaces were too complex and were not accurately oriented. The original program incorporated PCA analysis to automatically orient each pubic symphysis. Since the sternal rib end encompasses more varied and complex morphology than the pubic symphysis, this PCA analysis did not correctly orient each rib. Therefore, Detelina Stoyanova, creator of the original *forAge* script, generated a custom version of *forAge* for this analysis in which the PCA analysis was removed from the script. The custom *forAge* allowed for the user to manually orient the surface model prior to import into the program. Therefore, each rib was manually oriented where the x-axis was along the maximum length, the y-axis was orthogonal to the x-axis, and the z-axis measured depth of the pit (Figure 7).

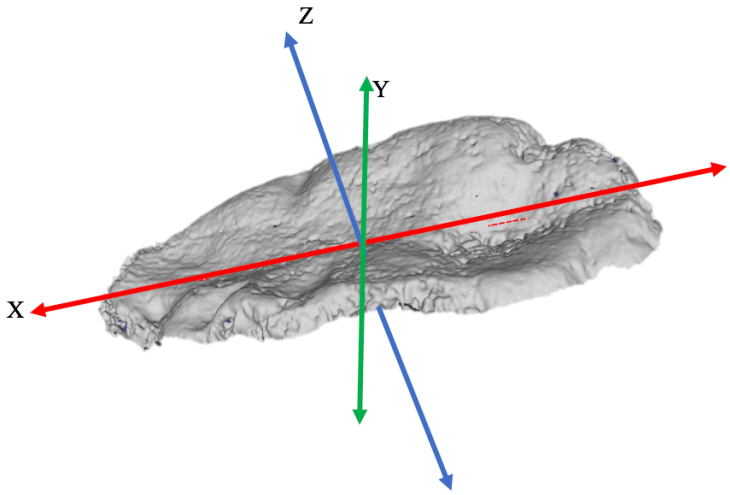

Figure 7. Oriented right, fourth rib from individual D19-2012.

This research utilized the custom *forAge* program to calculate raw SAH and BE scores from surface scans of the sternal extremity of the rib. These shape scores, which quantify the surface morphology of the sternal rib end, were recorded and used in subsequent statistical analyses for age-at-death estimation.

Statistical Analysis. The statistical analysis section consists of five parts: descriptive statistics, calculation of shape scores, regression-based age-at-death, analysis of phase-based age-at-death, and comparison of the phase-based and regression-based age-at-death methods (Figure 2). All statistical analyses were performed in R and were tested at a 95% confidence interval.

The first step of this statistical analysis was collection of basic descriptive statistics for the BE and SAH shape scores. This included an analysis of the distribution for the BE scores and SAH scores using the Shapiro-Wilk test. The Shapiro-Wilk test of normality tests the hypothesis that the dataset is normally distributed. Therefore, a p-value less than 0.05 rejects the hypothesis of a normal distribution, suggesting the data is not normally distributed (Madrigal 2012).

The second step of statistical analysis examined the process in which the BE and SAH shape scores were calculated. Since the custom *forAge* has never been tested before, it was necessary to assure that the BE and SAH shape scores generated between the two programs (original vs. custom) were not significantly different. Therefore, the shape scores from the original *forAge* were compared to the scores from the custom *forAge*.

Twenty-nine ribs did not work in the original version of *forAge*, therefore, only the remaining 51 were subjected to analysis in both programs. A paired t-test was performed comparing the means of the BE and SAH scores between the original and custom *forAge* program. The paired t-test tests the hypothesis that there is no difference in means of the shape scores between the two versions of the program. Therefore, a p-value less than 0.05 rejects the null hypothesis of no difference, indicating that the means are different. Additionally, Pearson's Correlation coefficients were calculated between the scores from the two programs.

The third step of statistical analysis generated the regression-based age-at-death estimation technique. The custom version of *forAge* was used to generate the shape scores for regression analysis. The shape scores from 80 rib surfaces and the known age-at-death for each individual were used in linear regression analysis. To maintain consistency, this study included the same regression analyses as the original pubic symphysis publications (Slice and Algee-Hewitt 2015, Stoyanova et al. 2015, Stoyanova et al. 2017). For all regression analyses, known age was the dependent variable (Y) and the shape scores were the independent variable(s) (X). A total of 12 regression formulae were created. First, each shape score (BE and SAH) was run in a univariate regression, then the scores were combined in a multivariate regression, similar to the publications examining the pubic symphysis (Slice and Algee-Hewitt 2015, Stoyanova et al. 2015). Next, both shape measures were run in a multivariate interaction formula. This

interaction equation was not used in the original pubic symphysis publications, but it was incorporated here with the hope of better understanding how the shape scores interact.

The basic assumption of linear regression is that the dataset is normally distributed (Madrigal 2012). Therefore, if the data is not normally distributed, a basic assumption of the linear regression model is violated. To meet the assumption of normality, each equation was also log transformed in two ways: first only the shape scores were transformed then both shape scores and age were transformed. The significance values at the p=0.05 alpha level, R^2 values, and x-validated Root-Mean-Squared-Errors (RMSE) were assessed for each regression equation. Values that fell below a p-value of 0.05 were considered significant. The R^2 values dictate what percentage of the values in the dataset fall on the regression line (Madrigal 2012). A perfect R^2 value is 1, or 100% of the values fall on the regression line. The ribs used to generate the regression equations were subjected to a leave-one-out cross-validation analysis in which one rib was excluded and new regression formulae were generated from the remaining ribs in the data set. Then the age-at-death was estimated for the excluded individual using the new regression formula generated from the remaining individuals in the dataset. Root-Mean-Squared-Error (RMSE) were calculated for each of these new equations. This leave-one-out cross-validation was used to generate a x-val RMSE estimate. This was preformed using the DiceEval package in R (Dupuy et al. 2015).

Prediction and confidence intervals were also calculated for each regression formula. The prediction intervals inform the distribution of the sample and dictate where a future predicted age-at-death estimate may fall. The confidence intervals dictate the range in which the true age-at-death is most likely to fall.

Next, the performance of the 12 regression formulae was examined using the İşcan-Loth casts. The exact age-at-death for each individual used to create the İşcan-Loth Rib Age Determination casts are unknown. Therefore, the shape scores from the casts were placed into each regression equation and the age-at-death estimates were compared to see if the regression-based age estimate fell within the range that the rib casts represented. For example, the BE shape score for the female phase 0 (F0) cast was plugged into the univariate BE regression formula, then the estimated age was compared the age-range associated with the F0 cast (>16). All regression-based age estimates were rounded up (e.g., 59.6 was considered 60) because all phase-based age ranges used whole numbers.

The fourth step of the statistical analysis examined the phase-based age-at-death estimation. The performance of the İşcan-Loth (1984a, 1985) and Hartnett (2010b) phase-based age-at-death estimation were tested using the 80 ribs with known ages. These two phase-based methods were examined for accuracy of phase-based age-at-death estimation compared to the known age-at-death. Then they were tested for intraobserver error, where the age-at-death estimation was examined for repeatability across three rounds scored by the same observer. Lastly, similar to the regression analysis described

above, x-validated RMSE values were calculated for both phase-based methods. Estimated phases and known age-at-death were used in generation of regression equations. These were then subjected to a leave-one-out cross-validation analysis where x-validated RMSE values were calculated.

Lastly, the fifth and final step of statistical analysis compared the phase-based and regression-based age-at-death estimation methodologies. The relationship of these age-at-death estimation methodologies to known age-at-death was assessed through calculation of correlation coefficients. Two types of correlation coefficients were calculated: Pearson's correlation and Spearman's Ranks correlation.

Both age-at-death and the regression-based age estimates are continuous variables. Therefore, Pearson's correlation was performed comparing the regression-based age-at-death estimates to known age-at-death. Since only age ranges are obtained from the phase-based methodologies, the phases, rather than age ranges, were correlated to the known age-at-death for each individual. Phases are ordinal variables while age-at-death is a continuous variable (Madrigal 2012). Therefore, a Spearman's Rank Correlation was performed comparing the phase-based phases to known age-at-death (Madrigal 2012). The two correlation coefficients for the phase-based and regression-based age-at-death estimates were then compared.

IV. RESULTS

The first research question asks if the morphology of the sternal extremity of the rib can be quantitatively measured to generate an objective age-at-death estimate. The second question addressed in this research asked if the regression analysis from morphological shape scores would provide a more accurate age-at-death estimation than traditional phase-based methods. The results of the statistical analyses which assessed these questions will be discussed in five steps: descriptive statistics, calculation of shape scores, regression-based age-at-death estimation, phase-based age-at-death estimation, and comparison of phase- and regression-based age-at-death estimation. All statistical analyses were performed in R and were tested at a 95% confidence interval.

Descriptive Statistics

Basic descriptive statistics were generated for both BE and SAH shape scores (Table 5). In addition, both shape scores were subjected to a Shapiro-Wilk normality test at the 95% significance level. The test-statistic for the BE scores was 0.7797 and the p-value of 0.0000 was significantly below 0.05, indicating that the hypothesis of normality was rejected. The dataset for the BE shape score was not normally distributed (Figure 8). The test-statistic for the SAH scores was 0.9766 and the p-value of 0.1495 was above 0.05. Therefore, the analysis for the SAH score failed to reject the hypothesis of normality and thus the distribution was normally distributed (Figure 9).

Table 5. Descriptive statistics for the BE and SAH shape scores.

Descriptive Statistics	BE score	SAH Score
Minimum	2.604	0.282
Maximum	174.427	1.451
Range	171.824	1.168
Sum	3080.796	61.912
Median	24.621	0.744
Mean	38.510	0.774
Standard Error of the Mean	4.114	0.027
CI Mean (0.95)	8.189	0.054
Variance	1353.940	0.059
Standard Deviation	36.796	0.244
Coefficient of Variation	0.955	0.315
Skewness	1.853	0.495
Kurtosis	6.235	3.004
Total Scores	80	80

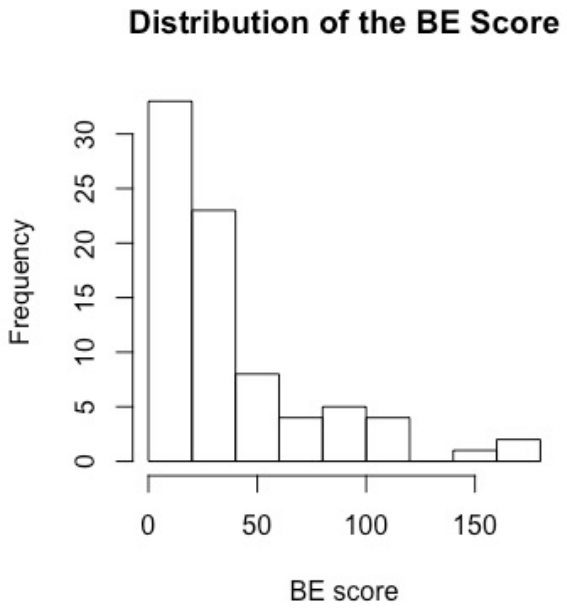

Figure 8. Distribution of the BE scores.

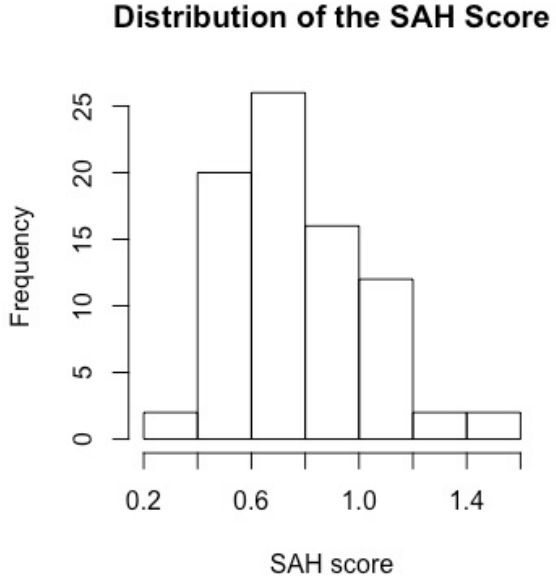

Figure 9. Distribution of the SAH scores.

Calculation of Shape Scores

A paired t-test was performed on the shape scores between the original *forAge* and the custom *forAge* programs. A total of 51 rib surfaces were compared because 29 rib surfaces did not work in the original *forAge* program. The paired t-test examined the hypothesis of no difference between the scores produced by the two programs. The t-test for the BE shape score produced a t-statistic of -0.297 and a p-value of 0.768. Therefore, the analysis failed to reject the null hypothesis, indicating that the BE scores between the original and custom *forAge* are not statistically different. The t-test for the SAH shape score produced a t-statistic of -1.653 and a p-value of 0.105. Therefore, the analysis failed to reject the null hypothesis, indicating that the SAH scores between the original and custom *forAge* are not statistically different. Pearson's correlation coefficients produced between the two versions of *forAge* were highly correlated with the BE correlation at 0.9093 and the SAH correlation at 0.9993. To maintain consistency, only the shape scores from the custom *forAge* were used in all subsequent analyses.

Regression-based Age-at-death Estimation

A total of 12 linear regression formulae were calculated. Table 6 displays all regression equations and associated p-values, r^2 values, and the x-val RMSE values. Additionally, figures 10-21 depict graphs for each regression formula including the regression line, confidence intervals, and prediction intervals. All formulae were significant with p-values well under p=0.05. Overall, the log transformed models

generated lower p-values and higher R-squared values than non-log transformed equations. The x-val RMSE values were lower than those reported in the original publications for the pubic symphysis, indicating a decreased error rate for age-at-death estimation from the compared the pubic symphysis (Slice and Algee-Hewitt 2015 and Stoyanova et al. 2015). The three equations using the univariate SAH score generated the lowest values of all 12 regression formulae with r-squared values between 0.09 and 0.16 and the x-val RMSE values between 16.6 and 16.9. Therefore, the equations for the SAH shape score appear to provide the worst fit. The Log Age vs. Log Multivariate Interaction equation has the highest R-squared and lowest x-val RMSE and thus, appears to provide the best fit.

Table 6. Regression formulae and their respective p-values, R^2 values, and x-validated Root Mean Squared Error (RMSE) values.

Description	Equations	P-value	R^2	x-val RMSE
BE	y= 0.18894*(BE)+ 50.69880	0.00245	0.1117	16.3805
Age vs. Log BE	y= 10.584*(log(BE))+ 23.414	0.00002	0.2098	15.1075
Log Age vs. Log BE	y=0.23304*(BE)+3.22012	0.00000	0.2413	15.5805
SAH	y= 26.147*(SAH)+ 37.740	0.00568	0.0940	16.8803
Age vs. Log SAH	y= 22.195*(log(SAH))+64.786	0.00157	0.1210	16.5714
Log Age vs. Log SAH	y=0.53034*(SAH)+ 4.14386	0.00020	0.1639	16.6504
Multivariate	y=((0.13210*BE)+(13.17772*SAH)) + 42.68961	0.00573	0.1255	16.3378
Age vs. Log Multivariate	y= ((10.755*(log(BE)))+(-0.615* (log(SAH)))+ 22.667	0.00012	0.2098	15.3145
Log Age vs. Log Multivariate	y=0.20857*(BE)+ 0.08798*(SAH)+ 3.32704	0.00002	0.2431	15.7797
Multivariate Interaction	y= ((1.0085*BE)+(38. 4656* SAH))+((BE*SAH)*(-0.8762))+ 20.5327	0.00017	0.2306	15.7635
Age vs. Log Multivariate Interaction	y= ((6.788*(log(BE)))+(39.266* (log(SAH)))+((log(BE)*log(SAH))*(-13.251)))+ 37.531	0.00004	0.2593	15.1056
Log Age vs. Log Multivariate Interaction	y=0.09794*(BE)+ 1.20014*((SAH)+(BE*SAH)*(-0.36954))+ 3.74154	0.00000	0.3343	15.5111

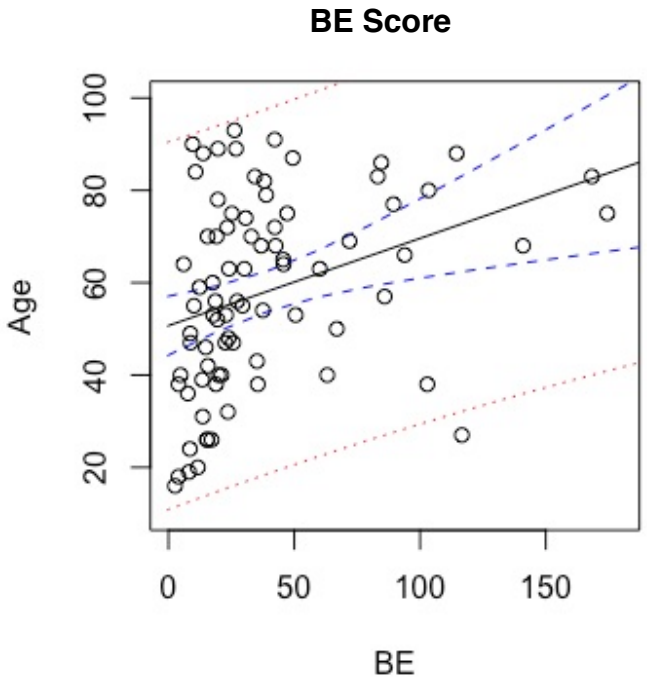

Figure 10. Regression plot of BE score vs. Age. The black solid line indices the regression line, the blue dashed lines indicate confidence intervals, and the red dotted lines indicate prediction intervals.

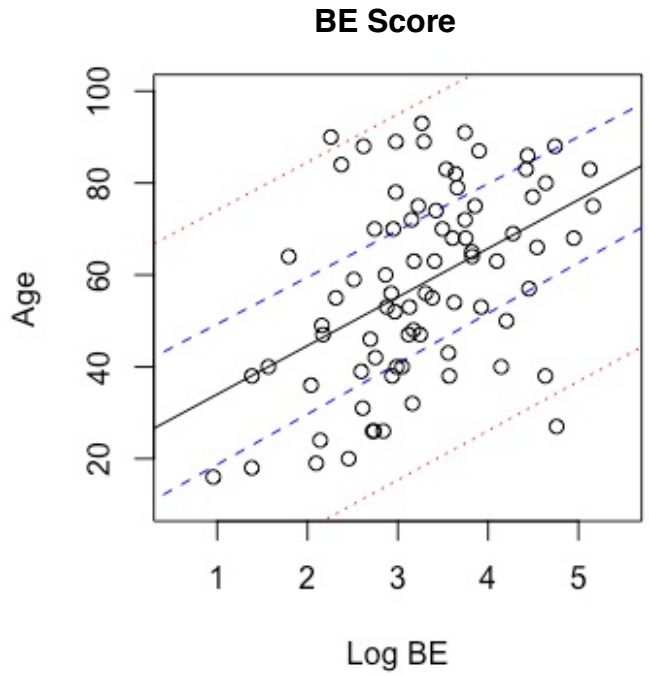

Figure 11. Regression plot of log BE score vs. Age. The black solid line indices the regression line, the blue dashed lines indicate confidence intervals, and the red dotted lines indicate prediction intervals.

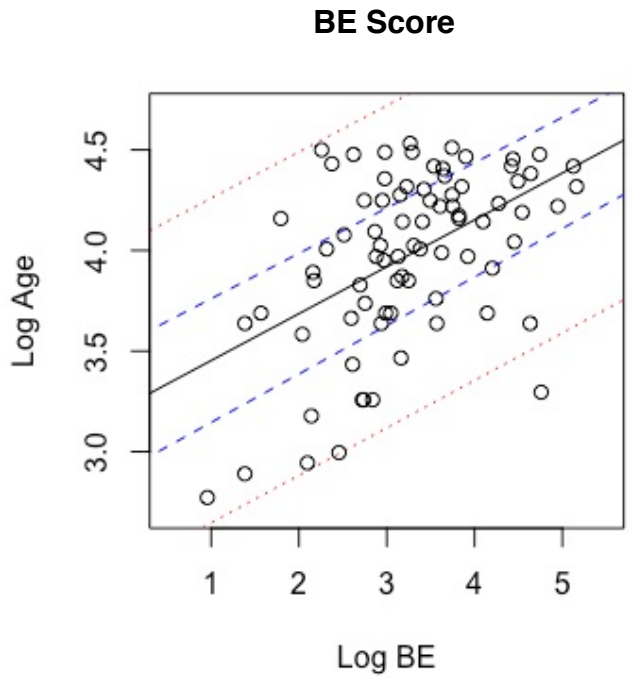

Figure 12. Regression plot of log BE score vs. log Age. The black solid line indices the regression line, the blue dashed lines indicate confidence intervals, and the red dotted lines indicate prediction intervals.

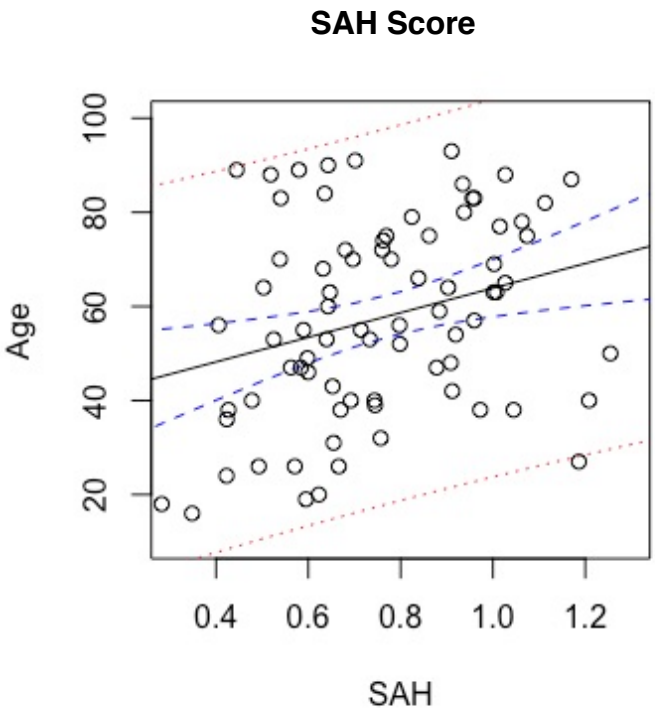

Figure 13. Regression plot of SAH score vs. Age. The black solid line indices the regression line, the blue dashed lines indicate confidence intervals, and the red dotted lines indicate prediction intervals.

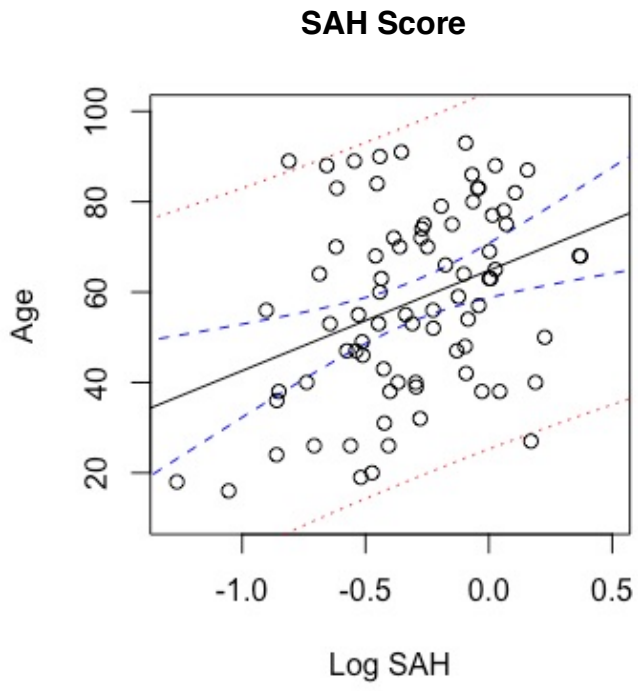

Figure 14. Regression plot of log SAH score vs. Age. The black solid line indices the regression line, the blue dashed lines indicate confidence intervals, and the red dotted lines indicate prediction intervals.

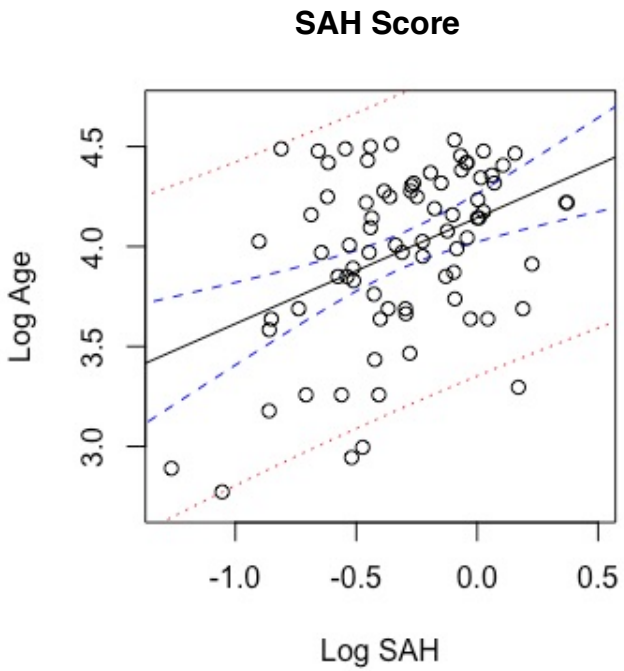

Figure 15. Regression plot of log SAH score vs. log Age. The black solid line indices the regression line, the blue dashed lines indicate confidence intervals, and the red dotted lines indicate prediction intervals.

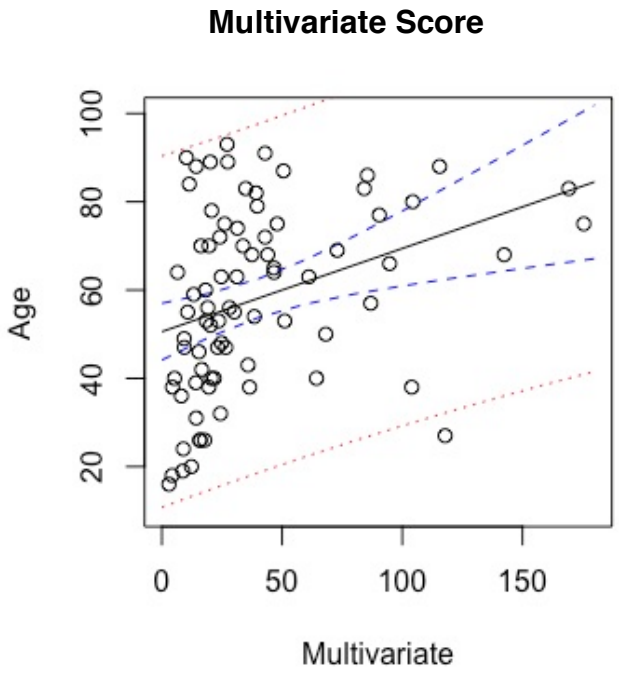

Figure 16. Regression plot of Multivariate vs. Age. The black solid line indices the regression line, the blue dashed lines indicate confidence intervals, and the red dotted lines indicate prediction intervals.

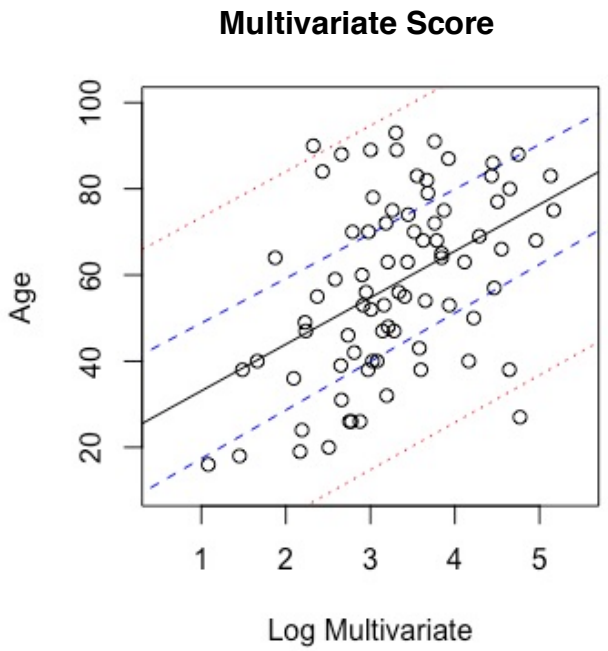

Figure 17. Regression plot of log Multivariate vs. Age. The black solid line indices the regression line, the blue dashed lines indicate confidence intervals, and the red dotted lines indicate prediction intervals.

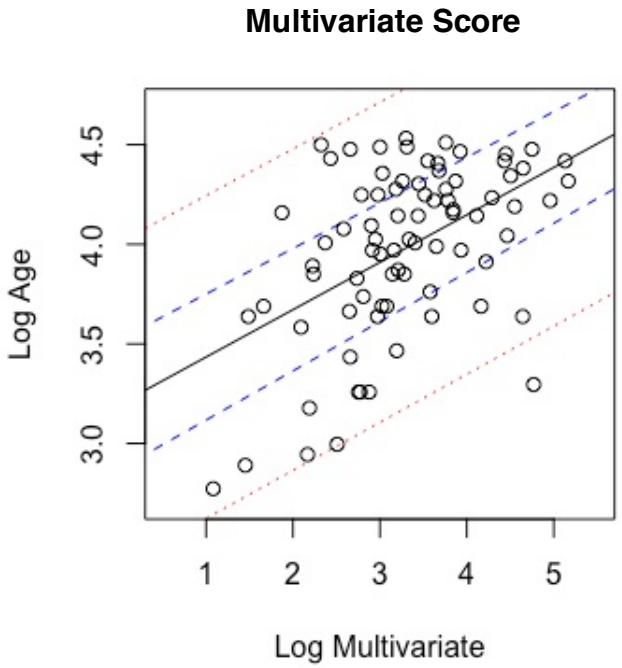

Figure 18. Regression plot of log Multivariate vs. log Age. The black solid line indices the regression line, the blue dashed lines indicate confidence intervals, and the red dotted lines indicate prediction intervals.

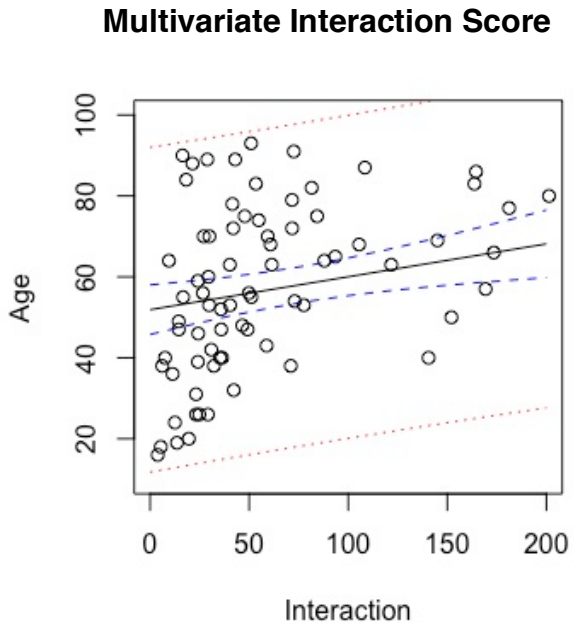

Figure 19. Regression plot of Multivariate Interaction vs. Age. The black solid line indices the regression line, the blue dashed lines indicate confidence intervals, and the red dotted lines indicate prediction intervals.

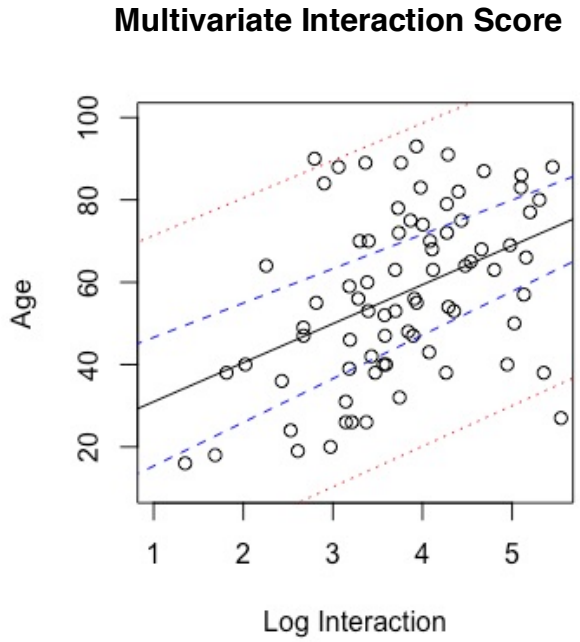

Figure 20. Regression plot of log Multivariate Interaction vs. Age. The black solid line indices the regression line, the blue dashed lines indicate confidence intervals, and the red dotted lines indicate prediction intervals.

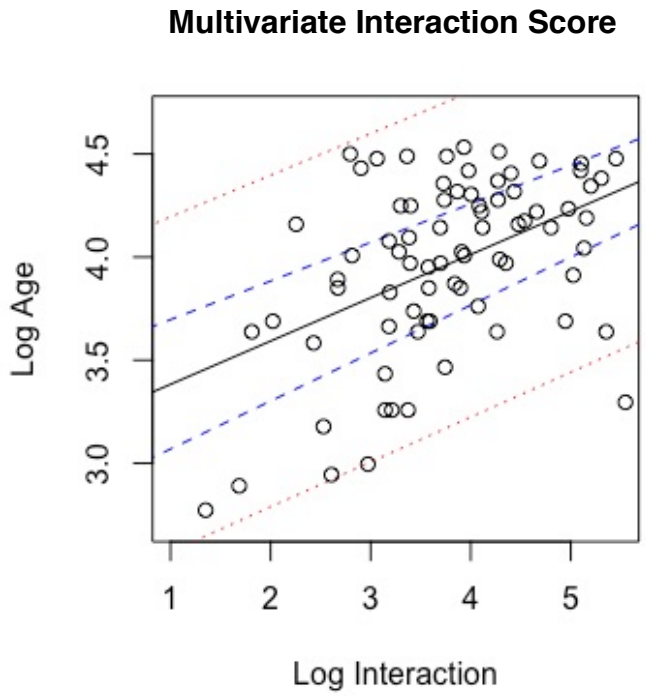

Figure 21. Regression plot of log Multivariate Interaction vs. log Age. The black solid line indices the regression line, the blue dashed lines indicate confidence intervals, and the red dotted lines indicate prediction intervals.

Performance of regression models. The İşcan-Loth Rib Age Determination casts were used to examine the performance of the 12 regression models. The regression-based age-at-death estimates for each rib cast were compared to see if the estimated age fell within the range that the rib casts represented (Appendix C and D). Results of this analysis are depicted in figures 20-27, where the bold vertical lines indicate the İşcan-Loth phase age-ranges and the black, red, and blue lines indicate which regression formula was used to estimate age at death. Graphs are separate by sex because the male and female casts are associated with different age ranges.

In general, non-log transformed formulae generated higher age estimates than log transformed equations. However, this was not true for the univariate SAH formulae, where age-at-death estimates between log-transformed equations and non-log-transformed equations were almost the same (Figures 22 and 23). Most regression equations overestimated the age-at-death for the casts representing the lower phases (i.e., younger ages). For the female casts, regression formulae estimated age-at-death within the appropriate age range for phases 4 to 7, which covers ages 24-83 (Figures 22, 24, 26, and 28). Female phases 0-3 and 8 had very few estimated ages that fell within the appropriate phase age-ranges. For males, most regression formulae estimated age-at-death within the appropriate age range for phases 5 to 8, which represent ages 28-85 (Figures 23, 25, 27, and 29).

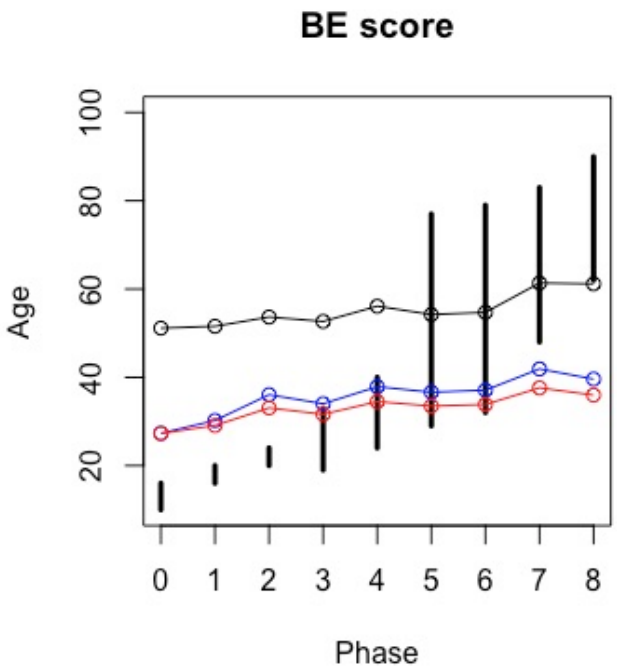

Figure 22. Plot of BE score regression-based age-at-death estimation for the Female İşcan-Loth Casts. The bold vertical lines indicate the İşcan-Loth phase age ranges, the black horizontal line indicates the average age estimation for BE vs. Age, the blue line indicates the average age estimation for Log BE vs. Age, and the red line indicates the average age estimation for Log BE vs. Log Age.

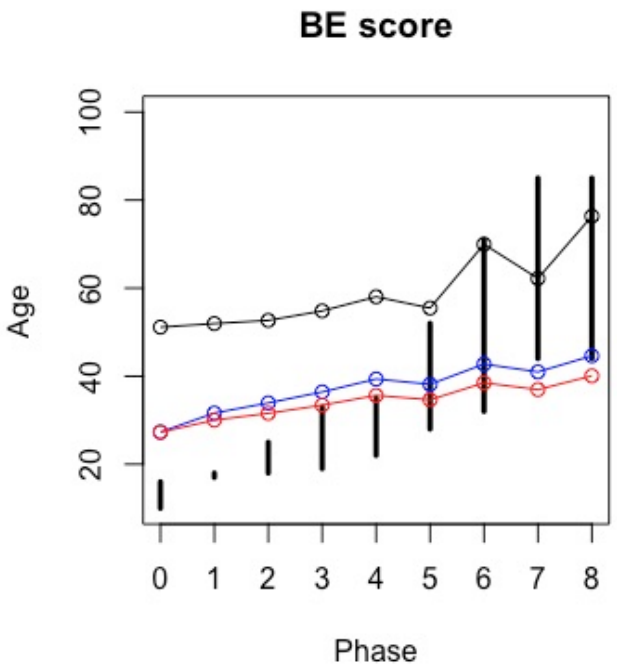

Figure 23. Plot of BE score regression-based age-at-death estimation for the Male İşcan-Loth Casts. The bold vertical lines indicate the İşcan-Loth phase age ranges, the black horizontal line indicates the average age estimation for BE vs. Age, the blue line indicates the average age estimation for Log BE vs. Age, and the red line indicates the average age estimation for Log BE vs. Log Age.

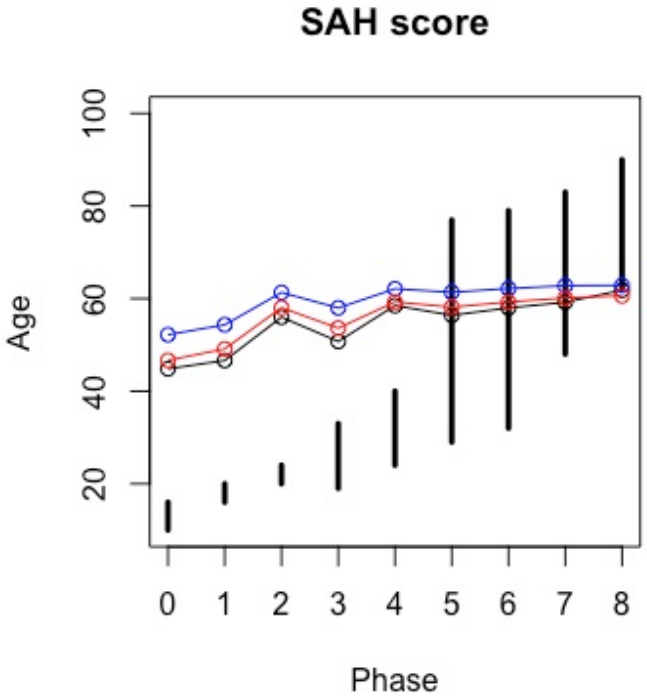

Figure 24. Plot of SAH score regression-based age-at-death estimation for the Female İşcan-Loth Casts. The bold vertical lines indicate the İşcan-Loth phase age ranges, the black horizontal line indicates the average age estimation for SAH vs. Age, the blue line indicates the average age estimation for Log SAH vs. Age, and the red line indicates the average age estimation for Log SAH vs. Log Age.

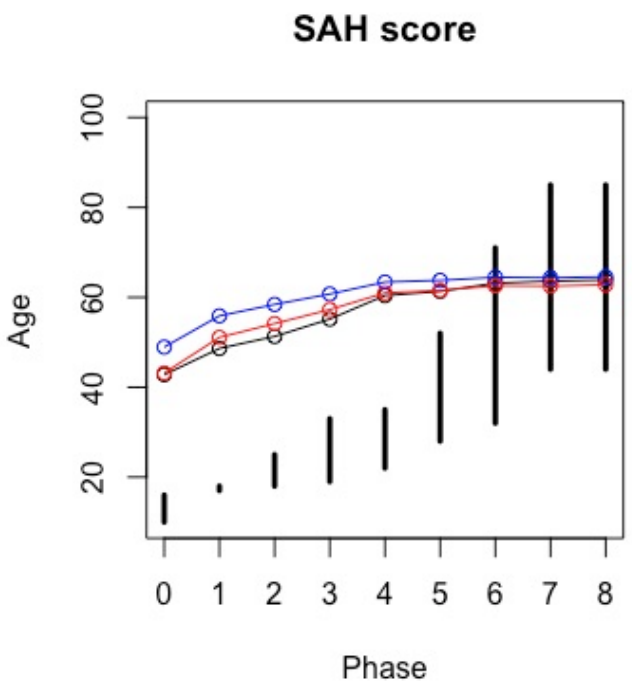

Figure 25. Plot of SAH score regression-based age-at-death estimation for the Male İşcan-Loth Casts. The bold vertical lines indicate the İşcan-Loth phase age ranges, the black horizontal line indicates the average age estimation for SAH vs. Age, the blue line indicates the average age estimation for Log SAH vs. Age, and the red line indicates the average age estimation for Log SAH vs. Log Age.

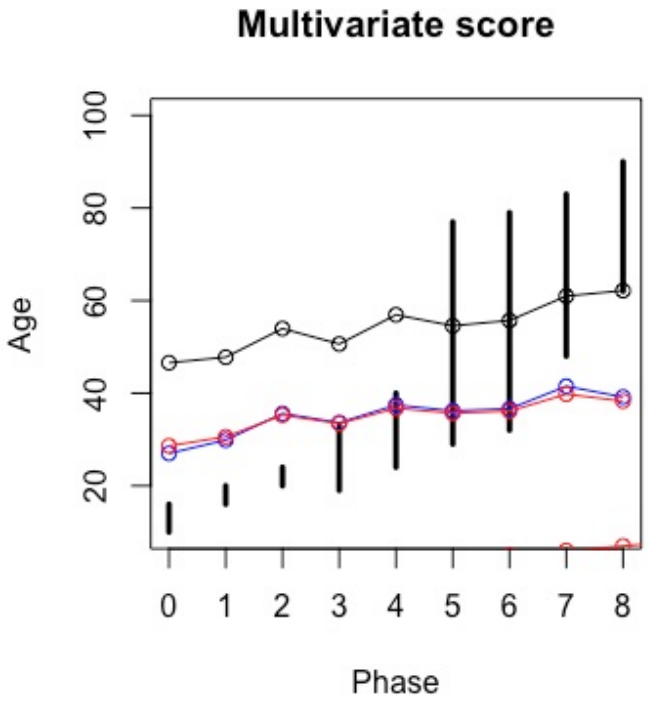

Figure 26. Plot of Multivariate score regression-based age-at-death estimation for the Female İşcan-Loth Casts. The bold vertical lines indicate the İşcan-Loth phase age ranges, the black horizontal line indicates the average age estimation for Multivariate vs. Age, the blue line indicates the average age estimation for Log Multivariate vs. Age, and the red line indicates the average age estimation for Log Multivariate vs. Log Age.

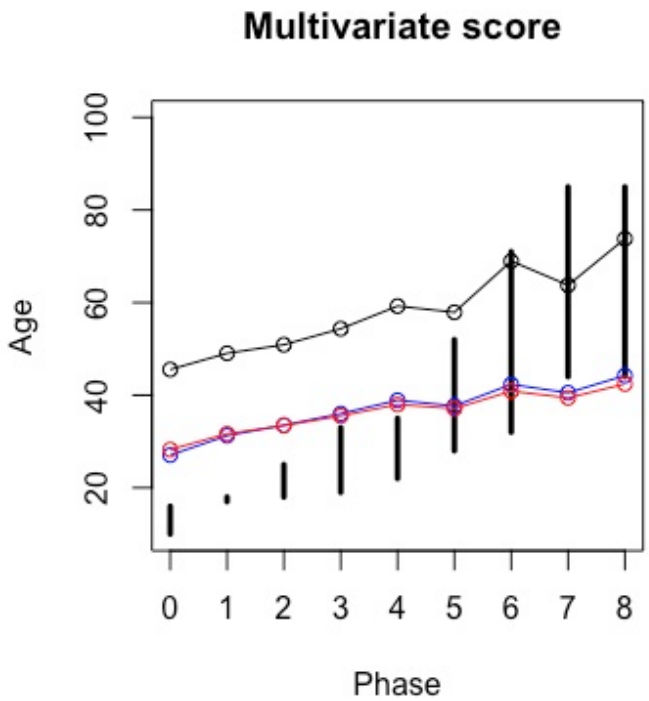

Figure 27. Plot of Multivariate score regression-based age-at-death estimation for the Male İşcan-Loth Casts. The bold vertical lines indicate the İşcan-Loth phase age ranges, the black horizontal line indicates the average age estimation for Multivariate vs. Age, the blue line indicates the average age estimation for Log Multivariate vs. Age, and the red line indicates the average age estimation for Log Multivariate vs. Log Age.

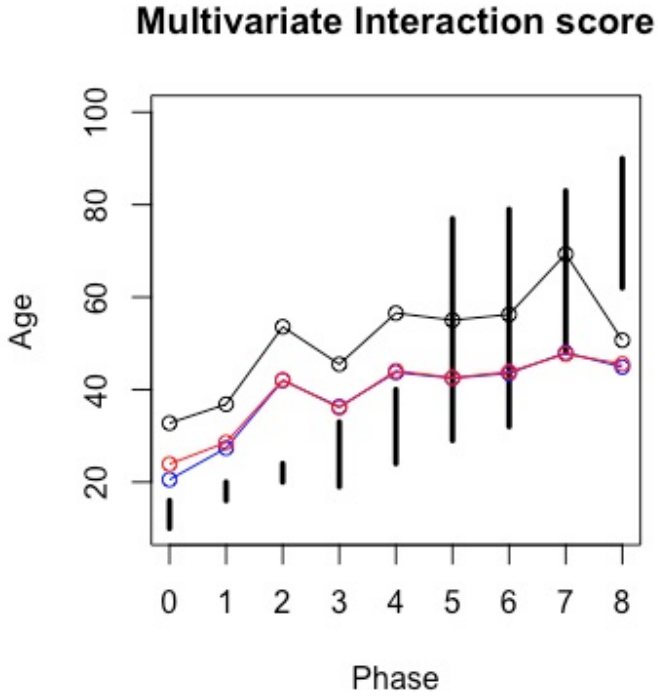

Figure 28. Plot of Multivariate Interaction regression-based age-at-death estimation for the Female İşcan-Loth Casts. The bold vertical lines indicate the İşcan-Loth phase age ranges, the black horizontal line indicates the average age estimation for Multivariate Interaction vs. Age, the blue line indicates the average age estimation for Log Multivariate Interaction vs. Age, and the red line indicates the average age estimation for Log Multivariate Interaction vs. Log Age.

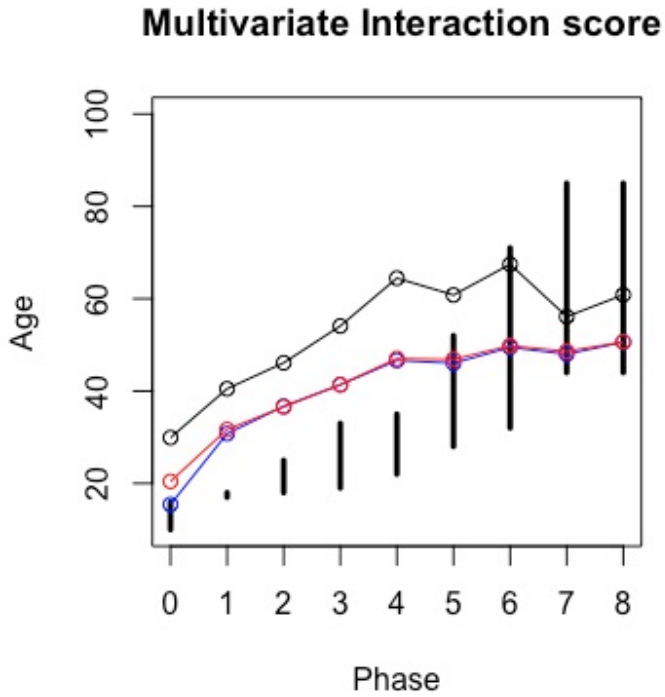

Figure 29. Plot of Multivariate Interaction regression-based age-at-death estimation for the Male İşcan-Loth Casts. The bold vertical lines indicate the İşcan-Loth phase age ranges, the black horizontal line indicates the average age estimation for Multivariate Interaction vs. Age, the blue line indicates the average age estimation for Log Multivariate Interaction vs. Age, and the red line indicates the average age estimation for Log Multivariate Interaction vs. Log Age.

Analysis of Phase-based Age-at-death Estimation

Phase assessments were collected for each of the 80 scanned ribs at three separate times. The percent correct was defined by the number of individuals whose known age-at-death fell within the correct phase-based age range divided by the total individuals assessed. The percent correct was calculated for each of the three rounds in which phases were collected. Then these percentages were averaged across all three rounds. In this study, the İşcan-Loth (1984a,1985) method provided a higher percentage of correct age-at-death estimates than the Hartnett (2010b) method for each of the three rounds (Table 7).

Table 7. Percent of correct phase-based age-at-death estimations for three rounds

Sex	Method	R1	R2	R3	Average
F	İşcan-Loth	88%	85%	91%	88%
	Hartnett	71%	62%	59%	64%
M	İşcan- Loth	80%	82%	84%	82%
	Hartnett	54%	48%	41%	48%

An analysis of intraobserver error was also assessed to examine repeatability of both phase-based methods. This was assessed through calculation of percentages for the number of ribs that were scored correctly in all 3 rounds, 2 of 3 rounds, 1 of 3 rounds, and 0 rounds (Table 8). Intraobserver error between rounds was greater for the Hartnett (2010b) method than the İşcan-Loth (1984a,1985) method. The İşcan-Loth method had the highest percentage scored correctly in all three rounds, where the Hartnett method had the highest percentages for age estimates that were not scored correctly in any round.

Table 8. Repeatability of phase-based age-at-death estimations across three rounds

Sex	Method	3/3	2/3	1/3	0
F	İşcan-Loth	76%	18%	0%	6%
	Hartnett	44%	18%	18%	21%
M	İşcan-Loth	73%	16%	9%	2%
	Hartnett	27%	24%	18%	31%

X-validated RMSE values were calculated for both phase-based methods. The x-validated RMSE values were 12.78955 and 11.12632 for the İşcan-Loth and Hartnett phase-based methods, respectively. These values are substantially lower than the values obtain through the objective scanning method described in this thesis.

Comparison of Phase-based and Regression-based Age-at-death Estimation

Both Pearson's Correlation and Spearman's Rank Correlation were performed to compare the phase-based phases and regression-based age-at-death estimates to known age-at-death. The results are depicted below (Figure 30). Overall, the phases from the phase-based methods were more highly correlated to the known age-at-death than the point age estimates generated from the 12 regression formulae. The Hartnett phase-based method had a higher correlation (r=0.65) to known age-at-death than the İşcan-Loth phase-based method (r=0.56). For the regression-based correlation coefficients, the univariate BE and SAH provided the lowest correlations to known age-at-death (r=0.33 and r=.31, respectively). The highest regression-based correlation coefficients were

reported for the multivariate interaction formula (r=0.48), the Age vs. Log BE equation (r=0.46), and the Age vs. Log Multivariate Interaction equation (r=0.46).

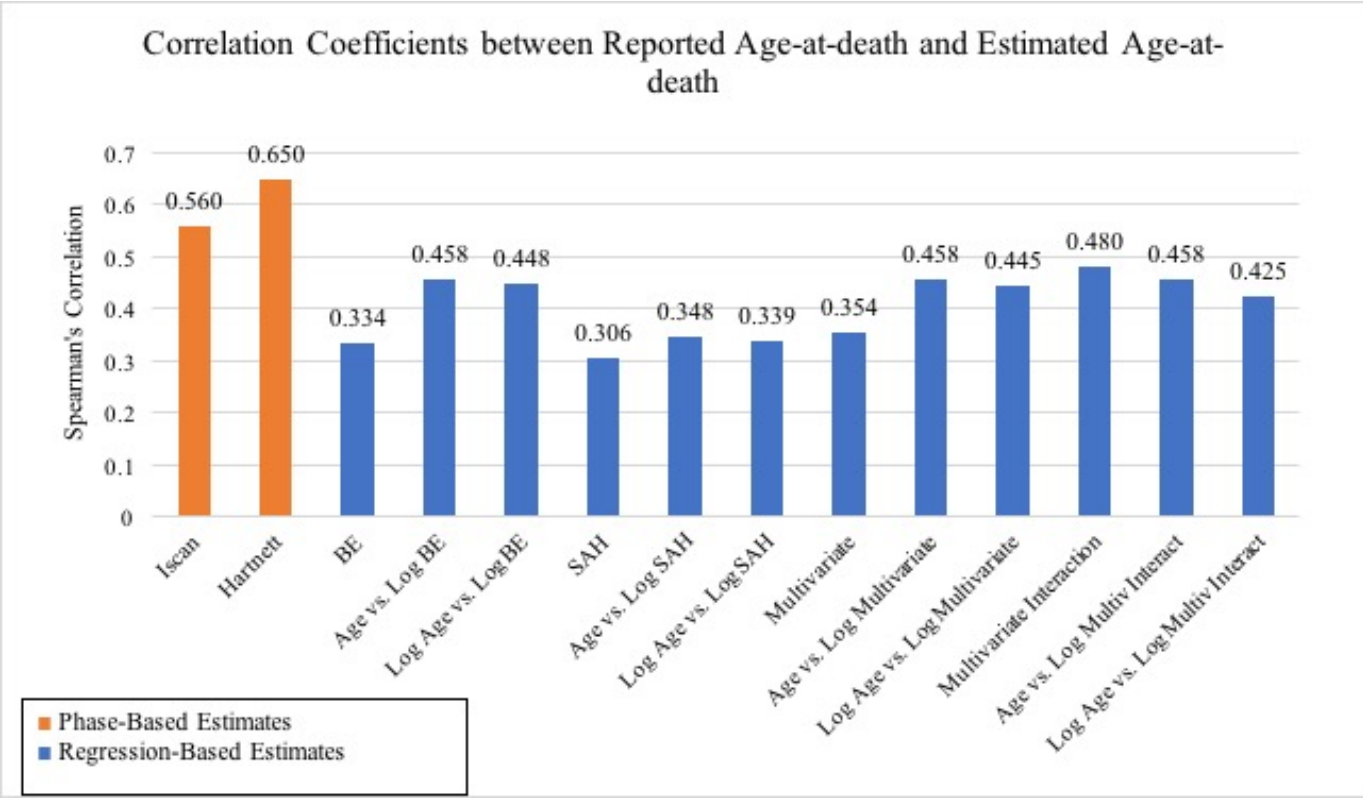

Figure 30. Correlation Coefficients between known age-at-death and phase-based phases and regression-based estimated age-at-death.

V. DISCUSSION

This study expanded on the previous research by Slice and Algee-Hewitt (2015) and Stoyanova et al (2015) who generated a novel technique of quantification of surface morphology of the pubic symphysis for objective age-at-death estimation. In this case, the pubic symphysis was exchanged for the sternal extremity of the rib and two research questions were addressed. The first research question examined if the SAH (Slice and Algee-Hewitt) and BE (Bending Energy) shape scores can quantitatively measure the morphology of the sternal rib end and, further, if the shape scores can be used in regression analysis to generate an objective age-at-death estimate. The second research question inquired if the objective regression-based equations provide more accurate age-at-death estimations than subjective phase-based age-at-death estimations. This discussion will critically examine the statistical results presented above and address the methodological implications that may have influenced those results. Finally, the discussion will summarize future directions to expand on this research.

Statistical Results

Regression-based age-at-death estimation. The goal of the linear regression analysis was to generate a representative group of formulae, including univariate, multivariate, multivariate interaction, and log transformed equations, to determine the best way to obtain an accurate and reliable age-at-death estimation from SAH and BE

shape measures. To maintain consistency, this study included the same regression analyses as the original publications (Slice and Algee-Hewitt 2015, Stoyanova et al. 2015, Stoyanova et al. 2017). Since the Shapiro-Wilk test of normality for the shape scores showed that the BE score was not normally distributed, a basic assumption of linear regression was violated. Thus, the age-at-death and the shape scores were log transformed prior to regression analysis with the goal of obtaining a sample data set that was normally distributed. This study also included an additional multivariate interaction equation. This interaction equation was generated by expanding the multivariate equation with addition of an equation in which the two shape scores were multiplied. Addition of the interaction explores how the effect of the BE shape score on age differs for different SAH values and vice versa.

All twelve regression formulae were significant at the p=0.05 alpha level. R-squared values ranged from 0.094 to 0.334, where most were above 0.20. The x-val RMSE values ranged between 15.11 and 16.88, all of which were lower than those reported by Slice and Algee-Hewitt (2015) and Stoyanova et al. (2015) but fall close to those reported in the more recent article in which the original datasets were expanded (Stoyanova et al. 2017). In general, the log-transformed formulae had higher R-squared values and lower x-val RMSE values than the non-log-transformed models. A Shapiro-Wilk normality test of the log-transformed BE values showed a t-statistic of 0.9912 and a p-value of 0.8049. This test failed to reject the hypothesis of normality thus showing the log-transformed BE values are normally distributed. Therefore, the log-transformation

was successful in meeting the basic assumption of normality for the linear regression analysis. The highest R-squared values and lowest RMSE values were reported for the Log Age vs. Log Multivariate Interaction formula, followed by the Age vs. Log Multivariate Interaction, and the Log Age vs. Log Multivariate formulae. This suggests that these equations provide the best model for age-at-death estimation using the BE and SAH shape scores. The three formulae using the univariate SAH score generated the lowest R-squared and highest x-val RMSE values, suggesting that the univariate SAH regression equations are poor performing models and provide the lowest association between age-at-death and the shape score.

The performance of the regression formulae was tested on the İşcan-Loth Rib Age Determination Casts. This analysis was inhibited by the fact that the true age-at-death for the individuals from which the casts were generated are unknown. Thus, the age-ranges associated with each cast were used for comparison to the estimated ages generated by the regression formulae. Results of this analysis regression formulae estimated age-at-death within the appropriate age range for phases 4 to phase 7 (i.e., ages 24-83) for females and phases 5 to 8 (i.e., ages 28-85) for males. Overall, the regression equations appeared to produce mediocre age-at-death estimations when tested on the İşcan-Loth Rib Age Determination Casts. However, these İşcan-Loth phases, and associated age ranges, represent a very wide range of age. For example, together female phases 4 to 7 represent an age range (24-83 years) that covers most of the ages in the sample used in this study. Similarly, phase 0-5 for both males and females cover ages 16-40, where the

sample used in this study is severely lacking. Thus, although the regression-based age-at-death estimates did not appear to work well for the İşcan-Loth phases below 4 for females and 5 for males, it may be a result of the sample used to generate the regression formulae and the extremely wide age ranges for phases 4 to 8.

Analysis of phase-based age-at-death estimation. Performance tests of the phase-based methods indicated that the İşcan-Loth method for both males and females better estimated age-at-death than the Hartnett (2010b) method. The estimated İşcan-Loth phases correctly encompassed the known age-at-death 80-91% of the time, while the Hartnett estimated phases correctly encompassed the known age-at-death 41-71% of the time (Table 7). However, a considerable amount of intraobserver error was observed for the Hartnett phase-based method. When the two phase-based methods were tested for repeatability across three rounds, the Hartnett method produced a high percentage (21%-31%) of incorrect age-at-death estimation consistently across all three rounds (Table 8). Conversely, the İşcan-Loth method produced high percentages of correct age-at-death estimation across three rounds (Table 8). The high rate of error for repeatability for the Hartnett method and the disjunction in the repeatability assessment for both phase-based age-at-death estimation methods suggests a general high rate of error for the phase-based methods.

Comparison of phase-based vs. regression-based age-at-death estimation. Comparison of Pearson's Correlation and the Spearman's Rank Correlation coefficients between the known age-at-death and estimated age-at-death from the phase-based and

regression-based methods produced a clear delineation between the two phase-based methods and each of the twelve regression-based equations. The phase-based methods produced correlation coefficients between r=0.56 and r=0.65, while all correlation coefficients for the regression-based methods were below r=0.48 (Figure 28). It was expected that the univariate SAH regression equations showed some of the lowest correlation values to age-at-death because these regression equations had the lowest associated r-squared values and the highest x-validates RMSE values. However, it was surprising that the regression equation with the highest r-squared values and the lowest x-validates RMSE values (Log Age vs. Log Multivariate Interaction) did not have the highest correlation coefficient (r=0.43). Additionally, phase-based X-validated RMSE values (11.13 and 12.79) were lower than those reported by the regression-based equations (ranged from 15.11 to 16.88).

Overall, the phase-based methodologies show a stronger relationship to known age-at-death than the regression-based age-at-death estimations to known age-at-death. The phase-based methodologies provided lower error estimates than the regression-based equations. This suggests that the traditional phase-based age-at-death estimation still out-perform the new regression-based age-at-death estimation generated in this study.

Methodological Implications

The poor performance of the objective regression-based age-at-death estimation may be best explained by several methodological implications.

Sample. This study aimed to obtain a sample representative of a range of ages in which morphological changes of the sternal extremity of the rib are prevalent. However, it was not possible to obtain ribs lacking post-mortem damage and observable pathology for several age brackets. Therefore, the sample for this research does not include females below 35 years. Also, the 20-24 age bracket only has two of a possible three males and the 90-94 age bracket only has two males and one female. The missing individuals from the 90-94 age bracket does not drastically affect the sample because there is little change in rib morphology among older age groups.

The final sample used to generate the regression formulae contained more individuals over the same of 35 years than individuals below 35 years. Additionally, the sample contained more males than females. This may explain the tendency for inaccurate age-at-death estimations for individuals below the age of 35. Future studies should seek to gain a more representative sample of the 15-35 age group, especially when research states that most of the rapid morphological changes in the rib occur during the teenage and young adult years (İşcan 1984a). Future studies may also cap the sample at about 75 years because there is little change in rib morphology among older age groups (e.g., over 75 years). Furthermore, the regression formulae could be improved through representative samples of both males and females.

MicroCT vs. surface scans. One major difference between this research and the original research on the pubic symphysis was the use of CT imaging rather than laser surface scans for collection of point-cloud data (Slice and Algee-Hewitt 2015). MicroCT

imaging was chosen because the alternative imaging technique (laser scanning) does not completely capture depth and complex surfaces, such as the deep pits and ossified cartilage present in many rib ends of older individuals. Major trade-offs to using the microCT imaging technique include the excess of data collected and the amount of time to generate the final surface model. Future studies may seek to find alternative ways to capture the surface morphology of the rib in which the amount of data and time it takes to capture the data is reduced.

Model editing. MicroCT imaging collects more data than surface laser scans. Thus, excess data, such as the trabeculae, had to be removed prior to import into *forAge*. The steps to generate a clean surface model included the manual editing of each individual rib (Figure 2). Further editing was performed if there was a large amount of ossified cartilage in the pit of the rib. In such cases, the cartilage in the pit was removed in Avizo 9.4, prior to removal of excess trabecular data and export in Meshlab v. 2016.12. The process of removing excess data adds a degree of subjectivity and a significant increase in time to this method. It is unknown how manual editing and removal of data from a surface model can change the shape scores calculated from the rib surface. Future studies may try to compare surface model editing between two different observers and between the same observer at different times to assess if the different post-processing of the models creates a significantly different model. Future studies may also seek to streamline the editing process to generate a standardized workflow, which in turn may decrease time and the added subjectivity of data removal.

Shape scores. The SAH and BE shape scores were originally generated to quantify the surface topography of the pubic symphysis. Just as with the pubic symphysis, the surface morphology of the sternal extremity of the rib changes through life. Generally, the pubic symphysis begins with a complex undulating surface morphology, then it flattens and simplifies, then becomes depressed and irregular (Todd 1920, Brooks and Suchey 1990). The sternal extremity of the rib begins with a rather simple, flat surface, then progressively the pit deepens and the rim morphology becomes increasingly irregular as age increases (İşcan and Loth 1984a). Although both skeletal indicators have differing trends in surface morphological change through life, general changes such as surface depression, irregular topography, and the general oval shape can be compared. Thus, the shape scores produced for the pubic symphysis were assumed to work well for sternal rib morphology. However, this assumption was not critically evaluated.

Two major differences between the rib and the pubic symphysis are the degree of complexity and the depth of the pit. It is more likely to observe complex morphology on the rib due to formation of ossified cartilage. This is normally associated with older individuals; however, it can also form in younger individuals due to trauma or pathology creating a large amount of variation in rib morphology (Hartnett 2010b). The SAH score was generated to "quantify the surface complexity of the pubic symphysis" (Slice and Algee-Hewitt 2015:841), thus was assumed to do the same for the sternal rib end. However, the original authors discussed a major shortcoming to the SAH score that "the

spatial structure of the data is not taken into account and similar results can be returned for different morphological expressions simply because they have the same variance" (Stoyanova et al. 2015:4). Therefore, it is possible that the SAH score could not differentiate the complex variation in rib end surface morphology and thus produced many similar SAH scores. This may be supported by the lowest R-squared and highest x-val RMSE values for the regression equations involving the SAH scores.

Similarly, the depth of the pit was assumed to be measured best by the BE score. It was believed that the deeper the pit, the more energy needed to bend the "infinitely thin, flat metal plate" (Stoyanova et al. 2014:4) against the rib surface morphology, and thus, the greater the BE score. However, this study did not include an in-depth analysis of how the BE score measured the depth of the pit, therefore it is unknown if pit depth was accurately incorporated into the quantification of the surface morphology. Overall, future studies may seek to critically consider how well the SAH and BE scores measured the shape and morphology of the sternal rib end.

Lastly, the most recent publication by the original authors discussed the addition of a third shape measure for the pubic symphysis, which measured the ventral curvature (VC) (Stoyanova et al. 2017). This shape measure was not appropriate for the rib, but the publication did produce better results with the addition of more shape measures. This suggests that more scores for quantification of the surface morphology may improve the age estimation. Future studies may seek to examine a way to better quantify the pit depth in sternal rib ends.

6. CONCLUSION

This study aimed to expand on recent efforts in the forensic anthropology community to quantify and objectify methodologies. Slice, Algee-Hewitt, Stoyanova and colleagues generated the *forAge* program to apply their novel quantitative and objective technique for age-at-death estimation on the pubic symphysis. This study expanded their efforts and applied their methodology to the sternal rib end. Point cloud data from micro CT scans of sternal rib ends were imported in the *forAge* program, where shape scores from the original publications quantified the surface morphology. Twelve regression formulae were generated using the shape scores and the known age-at-death from each rib.

Results showed that this new regression-based method did not hold up when compared to the traditional phase-based age-at-death estimations. However, high intraobserver error rates for the phase-based methods suggest high rates of error in the subjective phase-based methodology. Therefore, this new, objective method of age-at-death estimation on the rib still shows promise and there are many avenues for improvement. Future studies may seek to incorporate a bigger, more representative sample size, a streamlined and automated editing process, and additional shape measures to better quantify the complex surface morphology of the sternal rib end.

APPENDIX SECTION

APPENDIX A

İşcan and Loth (1984a:1096-1099) rib phase descriptions.

Phase 0: the articular surface is flat or billowy with a regular rim and rounded edges. The bone itself is smooth, firm, and very solid.

Phase 1: There is a beginning amorphous indentation in the articular surface, but billowing may also still be present. The rim is rounded and regular. In some cases scallops may start to appear at the edges. The bone is still firm, smooth and solid

Phase 2: The pit is now deeper and has assumed a V-shaped appearance formed by the anterior and posterior walls. The walls are thick and smooth with a scalloped or slightly wavy rim with rounded edges. The bone is firm and solid

Phase 3: The deepening put has taken on a narrow to moderately U-shape. Walls are still fairly thick with rounded edges. Some scalloping may still be present but the rim is becoming more irregular. The bone is still quite firm and solid.

Phase 4: Put depth is increasing, but the same is still a narrow to moderately wide U. The walls are thinner, but the edges remain rounded. The rim is more irregular with no uniform scalloping pattern remaining. There is some decrease in the weight and firmness of the bone, however, the overall quality of the bone is still good.

Phase 5: There is little change in the put depth, but the shape in this phase is predominantly a moderately wide U. Walls show further thinning and the edges are becoming sharp. Irregularity is increasing in the rim. Scalloping pattern is completely gone and has been replaced with irregular bony projections. The condition of the bone is fairly good, however, there are some signs of deterioration with evidence of porosity and loss if density.

Phase 6: The pit is noticeably deep with a wide U-shape. The walls are thin with sharp edges. The rim is irregular and exhibits some rather long bony projections that are frequently more pronounced at the superior and inferior borders. The bone is noticeably lighter in weight, thinner, and more porous, especially inside the pit.

Phase 7: The pit is deep with a wide to very wide U-shape. The walls are thin and fragile with sharp, irregular edges and bony projections. The bone is light in weight and brittle with significant deterioration in quality and obvious porosity.

Phase 8: In this final phase the put is very deep and widely U-shaped. In some cases the floor of the put is absent or filled with bony projections. The walls are extremely thin, fragile, and brittle with sharp, highly irregular edges and bony projections. The bone is very lightweight, thin, brittle, friable, and porous. “Window” formation is sometimes seen in the walls.

APPENDIX B

Hartnett (2010b:1156) revised phase descriptions.

Phase 1: The pit is shallow and flat, and there are billows in the pit. The pit is shallow U-shaped in cross-section. The bone is very firm and solid, smooth to the touch, dense, and of good quality. The walls of the rim are thick. The rim may show the beginnings of scalloping.

Phase 2: There is an indentation to the pit. The pit is V-shaped in cross-section, and the rim is well defined with round edges. The rim is regular with some scalloping. The bone is firm and solid, smooth to the touch, dense, and of good quality. There is no flare to the rim edges; they are parallel to each other. The pit is still smooth inside, with little to no porosity. In females, the central arc, which manifests on the anterior and posterior walls as a semicircular curve, is visible.

Phase 3: The pit is V-shaped, and there is a slight flare to the rim edges. The rim edges are becoming undulating and slightly irregular, and there may be remnants of scallops, but they look worn down. There are no bony projections from the rim. There is porosity inside the pit. The bone quality is good; it is firm, solid, and smooth to the touch. The rim edges are rounded, but sharp. In many females, there is a build-up of bony plaque, either in the bottom of the pit or lining the interior of the pit, creating the appearance of a two-layer rim. An irregular central arc may be apparent.

Phase 4: The pit is deep and U-shaped. The edges of the pit flare outwards, expanding the oval area inside the pit. The rim edges are not undulating or scalloped but are irregular. There are no long bony projections from the rim, and the rim edges are thin, but firm. The bone quality is good but does not feel dense or heavy. There is porosity inside the pit. In some males, two distinct depressions are visible in the pit. In females, the central arc may be present and irregular; however, the superior and inferior edges of the rim have developed, decreasing the prominence of the central arc.

Phase 5: There are frequently small bony projections along the rim edges, especially at the superior and inferior edges of the rim. The pit is deep and U-shaped. The rim edges are irregular, flared, sharp, and thin. There is porosity inside the pit. The bone quality is fair; the bone is coarse to the touch and feels lighter than it looks.

Phase 6: The bone quality is fair to poor, light in weight, and the surfaces of the bone feel coarse and brittle. There are bony projections along the rim edges, especially at the superior and inferior edges, some of which may be over 1 cm long. The pit is deep and U-shaped. The rim is very irregular, thin, and fragile. There is porosity inside the pit. In some cases, there may be small bony extrusions inside the pit. In females, the central arc

is not prominent.

Phase 7: The bone is very poor quality, and in many cases, translucent. The bone is very light, sometimes feeling like paper, and feels coarse and brittle to the touch. The pit is deep and U-shaped. There may be long bony growths inside the pit. The rim is very irregular with long bony projections. In some cases, much of the cartilage has ossified and window formation occurs. In some females, much of the cartilage in the interior of the pit has ossified into a bony projection extending more than 1 cm in length.

Variant: In some males, the cartilage has completely or almost completely ossified. The ossification tends to be a solid extension of bone, rather than a thin projection. All of the bone is of very good quality, including the ossification. It is dense, heavy, and smooth. In these instances, bone quality should be the determining factor. There are probably other factors, such as disease, trauma, or substance abuse that caused premature ossification of the cartilage. When the individual is truly very old, the bone quality will be very poor. Be aware of these instances where a rib end may appear very old because of ossification of the cartilage but is really actually a young individual, which can be ascertained by bone quality. In these cases, consult other age indicators in conjunction with the rib end.

APPENDIX C

Age estimates for each regression equation for the female İşcan-Loth Rib Age Determination Casts. Bold indicates that the estimated age fell within the age-range for the cast.

Cast	Age Range	Estimated Age											
		BE	Age vs. Log BE	Log Age vs. Log BE	SAH	Age vs. Log SAH	Log Age vs. Log SAH	Multivariate	Age vs. Log Multivariate	Log Age vs. Log Multivariate	Multivariate Interaction	Age vs. Log Multivariate Interaction	Log Age vs. Log Multivariate Interaction
F0	>16	51.14	27.32	27.28	44.82	52.19	46.66	46.57	26.98	28.62	32.75	20.53	23.90
F1a	>16	51.32	28.89	28.24	45.74	53.37	47.99	47.16	28.54	29.65	34.73	24.36	26.39
F1b		51.81	31.56	29.95	47.52	55.31	50.27	48.40	31.20	31.50	38.92	30.34	30.75
F2a	16-20	53.58	35.93	32.97	55.98	61.32	58.03	53.89	35.48	35.16	53.42	41.87	42.02
F2b		53.74	36.18	33.16	55.98	61.32	58.03	54.01	35.74	35.34	53.76	42.08	42.17
F3a	20-24	53.17	35.24	32.48	52.11	59.02	54.93	51.66	34.84	34.37	48.58	38.76	38.34
F3b		52.15	32.78	30.77	49.36	56.97	52.31	49.56	32.40	32.48	42.39	33.85	33.82
F4a	24-40	52.94	**34.79**	**32.15**	52.28	59.13	55.07	51.58	**34.38**	**34.08**	48.11	**38.44**	**38.17**
F4b		59.29	**40.96**	**36.83**	64.69	65.08	63.49	62.28	**40.49**	**39.41**	64.97	49.01	49.98
F5a	29-77	**52.82**	**34.53**	**31.97**	**54.00**	**60.20**	**56.51**	**52.37**	**34.09**	**34.05**	**49.65**	**39.43**	**39.52**
F5b		**55.36**	**38.15**	**34.62**	**53.80**	**60.09**	**56.35**	**54.04**	**37.77**	**36.55**	**55.76**	**42.58**	**41.80**
F5c		**54.49**	**37.20**	**33.91**	**61.37**	**63.81**	**61.59**	**57.25**	**36.70**	**36.41**	**59.64**	**45.40**	**46.41**
F6a	32-79	**53.62**	**36.00**	**33.02**	**54.31**	**60.39**	**56.76**	**53.08**	**35.57**	**35.08**	**51.91**	**40.94**	**40.74**
F6b		**53.40**	**35.64**	**32.76**	**56.52**	**61.59**	**58.42**	**54.04**	**35.18**	**35.00**	**53.58**	**41.93**	**42.24**

(Continued) Age estimates for each regression equation for the Female İşcan-Loth Rib Age Determination Casts. Bold indicates that the estimated age fell within the age-range for the cast.

F6c		**57.14**	**39.63**	**35.77**	**63.15**	**64.51**	**62.63**	**60.00**	**39.16**	**38.30**	**63.26**	**47.70**	**48.61**
F7a	48-83	**63.04**	42.62	38.21	**56.18**	**61.42**	**58.17**	**60.61**	42.28	40.13	**73.17**	**47.54**	46.48
F7b		**59.69**	41.17	37.00	**62.25**	**64.16**	**62.12**	**61.33**	40.73	39.43	**65.50**	**48.44**	**48.89**
F8a		59.40	41.02	36.88	59.46	**63.00**	**60.41**	59.72	40.60	39.13	**65.40**	47.43	47.33
F8b	62-90	52.11	32.64	30.67	49.35	56.96	**52.29**	49.52	32.26	32.39	42.22	33.68	33.69
F8c		**72.04**	45.14	40.39	**76.65**	**68.62**	**69.09**	**77.22**	44.64	43.40	44.40	53.55	55.64
Percent Correct		45%	40%	40%	45%	50%	55%	45%	40%	40%	45%	45%	40%

APPENDIX D

Age estimates for each regression equation for the Male İşcan-Loth Rib Age Determination Casts. Bold indicates that the estimated age fell within the age-range for the cast.

Cast	Age Range	Estimated Age											
		BE	Age vs. Log BE	Log Age vs. Log BE	SAH	Age vs. Log SAH	Log Age vs. Log SAH	Multivariate	Age vs. Log Multivariate	Log Age vs. Log Multivariate	Multivariate Interaction	Age vs. Log Multivariate Interaction	Log Age vs. Log Multivariate Interaction
M0	>16	51.14	27.30	27.27	42.78	48.92	43.16	45.54	27.06	28.24	29.91	**15.44**	20.43
M1a	17-18	51.39	29.41	28.56	45.34	52.88	47.44	47.01	29.09	29.90	34.50	24.34	26.19
M1b		52.52	33.84	31.49	51.88	58.86	54.72	51.09	33.42	33.41	46.50	37.22	37.14
M2a	18-25	52.02	32.35	30.47	50.04	57.52	53.00	49.81	31.95	32.27	42.80	34.07	34.24
M2b		53.32	35.50	32.67	52.55	59.31	55.31	51.99	35.10	34.59	49.43	39.33	38.91
M3a	19-33	57.43	39.84	35.93	58.04	62.35	59.47	57.62	39.42	38.13	62.08	46.01	45.81
M3b		52.22	**33.01**	**30.92**	52.26	59.11	55.05	51.07	**32.57**	**32.91**	46.10	36.72	36.94
M4a	22-35	62.19	42.30	37.94	59.18	62.87	60.23	61.53	**41.91**	40.11	69.72	48.30	47.93
M4b		53.89	36.41	**33.32**	61.60	63.91	61.73	56.95	35.90	35.86	59.17	44.95	46.16
M5a		54.43	**37.12**	**33.85**	60.44	63.42	61.02	56.73	**36.63**	**36.30**	58.81	**44.96**	**45.79**
M5b	28-52	56.80	**39.39**	**35.58**	60.27	63.35	60.92	58.31	**38.94**	**37.94**	61.86	**46.53**	**46.89**
M5c		55.18	**37.97**	**34.49**	63.24	64.54	62.68	58.68	**37.46**	**37.07**	61.70	**46.64**	**47.88**
M6a		92.46	**48.23**	**43.23**	**65.91**	**65.50**	**64.14**	86.08	**47.86**	**45.55**	76.23	**53.71**	**53.62**
M6b	32-71	**62.67**	**42.49**	**38.09**	**63.85**	**64.77**	**63.02**	**64.22**	**42.05**	**40.56**	**67.41**	**49.75**	**50.28**
M6c		**54.77**	**37.53**	**34.15**	**59.70**	**63.11**	**60.56**	**56.61**	**37.06**	**36.54**	**58.72**	**44.95**	**45.54**

(Continued) Age estimates for each regression equation for the Male İşcan-Loth Rib Age Determination Casts. Bold indicates that the estimated age fell within the age-range for the cast.

M7a	44-85	**55.25**	38.04	34.54	**59.37**	**62.96**	**60.35**	**56.77**	37.58	36.89	**59.18**	**45.18**	**45.61**
M7b		**74.82**	**45.70**	40.89	**73.56**	**67.82**	**67.79**	**77.60**	**45.23**	43.74	**48.74**	**53.38**	**54.90**
M7c		**56.54**	39.19	35.42	**57.85**	**62.25**	**59.34**	**56.91**	38.76	37.63	**60.46**	**45.42**	**45.30**
M8a		**56.86**	39.43	35.61	**58.13**	**62.39**	**59.54**	**57.27**	39.01	37.83	**61.13**	**45.73**	**45.63**
M8b	44-85	**74.72**	**45.69**	40.87	**61.97**	**64.05**	**61.95**	**71.70**	**45.32**	43.08	**81.18**	**51.44**	**51.09**
M8c		**97.48**	**48.75**	43.73	**71.44**	**67.23**	**66.84**	92.38	**48.34**	**46.34**	40.18	**54.61**	**55.19**
Percent Correct		38%	48%	38%	43%	43%	43%	33%	52%	38%	33%	57%	57%

LITERATURE CITED

Baccino E, Ubelaker DH, Hayek LC, Zerilli A. 1999. Evaluation of seven methods of estimating age at death from mature human skeletal remains. J Forensic Sci 44:931–6.

Boldsen JL, Milner GR, Konigsberg LW, Wood JW. 2002. Transition Analysis: A New Method for Estimating Age from Skeletons. In Hoppa RD and Vaupel JW, editors. Paleodemography: Age Distributions from Skeletal Samples. Cambridge University Press:Cambridge. p 73-106.

Brooks S, Suchey JM. 1990. Skeletal age determination based on the OS pubis: a comparison of the Acsadi-Nemeskeri and Suchey-Brooks methods. Hum Evol 5:227–238.

Buckberry JL and Chamberlain AT. 2002. Age estimation from the auricular surface of the ilium: A revised method. Am J Phys Anthropol 119:231-239.

Christensen AM, Crowder CM. 2009. Evidentiary standards for forensic anthropology. J Forensic Sci 54(6):1211–1216.

Christensen AM, Passalacqua NV, Bartelink EJ. 2014. Age estimation. In: Christensen AM, Passalacqua NV, Bartelink EJ, editors. Forensic anthropology. Academic Press:San Diego. p 243-281.

Dedouit F, Bindel S, Gainza D, Blanc A, Joffre F, Rouge D. 2008. Application of the İşcan method to two- and three-dimensional imaging of the sternal end of the right fourth rib. J Forensic Sci 53:288–95.

Dedouit, F, Savall F, Mokrane FZ. 2014. Virtual anthropology and forensic identification using multidetector CT. Brit J Radiol 87:1036-1048.

Demsar U, Harris P, Brunsdon C, Fotheringham AS, McLoone S. 2013. Principal component analysis on spatial data: An overview. Ann Assoc Am Geogr 103:106-128.

Dupuy D, Helbert C, Franco J. 2015. DiceDesign and DiceEval: Two r packages for design and analysis of computer experiments. J Stat Software, 65(11), 1-38. URL http://www.jstatsoft.org/v65/i11/.

Fanton L, Gustin MP, Paultre U, Schrag B, Malicier D. 2010. Critical study of observation of the sternal end of the right 4th rib. J Forensic Sci. 55(2):467-472.

Garvin HM, Passalacqua NV. 2012. Current practices by forensic anthropologists in adult skeletal age estimation. J Forensic Sci. 57:427-433.

Hartnett, KM. 2010a. Analysis of age-at-death estimation using data from a new, modern autopsy sample—part I: Pubic bone. J Forensic Sci 55(5): 1145-1150.

Hartnett, KM. 2010b. Analysis of age-at-death estimation using data from a new, modern autopsy sample-part II: Sternal end of the fourth rib. J Forensic Sci 55(5): 1152-1156.

İşcan, MY, Loth SR, Wright RK. 1984a. Age estimation from the rib by phase analysis: white males. J Forensic Sci 29:1094–1104.

İşcan, MY, Loth SR, Wright RK. 1984b. Metamorphosis at sternal rib end: A new method to estimate age at death in white males. Am J Phys Anthropol 65:147–156.

İşcan, MY, Loth SR, Wright RK.1985. Age estimation from the rib by phase analysis: white females. J Forensic Sci 30:853–863.

İşcan, M Y, Loth SR, Wright RK 1987. Racial variation in the sternal extremity of the rib and its effect on age determination. J Forensic Sci 32(2):452-466.

Lovejoy CO, Meindl RS, Pryzbeck TR, Mensforth RP. 1985. Chronological metamorphosis of the auricular surface of the ilium: a new method for the determination of adult skeletal age at death. Am J Phys Anthropol 68:15–28.

Martrille L, Ubelaker DH, Cattaneo C, Seguret F, Tremblay M, Baccino E. 2007. Comparison of four skeletal methods for the estimation of age at death on white and black adults. J Forensic Sci 52(2):302–7.

MacAluso PJ, Lucena J. 2012. Test of a new components method for age-at-death estimation from the medial end of the fourth rib using a modern Spanish sample. Int J Legal Med126(5): 773-779.

Madrigal L. 2012. Statistics for Anthropology. Cambridge University Press: West Nyack, NY. p 1-278.

Mann RW. 1993. A method for siding and sequencing human ribs. J Forensic Sci 38:151-155.

Meena MC, Rani Y. 2014. Age estimation from the IV rib by the components method in Indian males. Aust J Forensic Sci 46(4): 463-470.

Merritt CE. 2014. A Test of Hartnett's Revisions to the Pubic Symphysis and Fourth Rib Methods on a Modern Sample. J Forensic Sci. 59(3):703-713.

Moskovitch G, Dedouit F, Braga J, Roug D, Rousseau H, Telmon N. 2010. Multislice computed tomography of the first rib: a useful technique for bone age assessment. J Forensic Sci 55(4): 865-870.

Nikita E. 2013. Quantitative assessment of the sternal rib end morphology and implications for its application in aging human remains. J Forensic Sci 58(2):324–329.

Oettle AC and Steyn M. 2000. Age estimation from sternal ends of ribs by phase analysis in South African Blacks. J Forensic Sci 45(5)1071-1079.

Özgür A, Ekin, Koçak A, Aktas S, Yemisçigil A. 2004. Intercostal variation for age estimation – are the standards for the right 4th rib applicable for other ribs? Coll Anthropol 2:267-272.

R Core Team. 2016. A Language and Environment for Statistical Computing. R Foundation for Statistical Computing, Vienna, Austria. URL https://www.R-project.org.

Russell KF, Simpson SW, Genovese J, Kinkel MD, Meindl RS, Lovejoy CO. 1993. Independent test of the fourth rib aging technique. Am J Phys Anthropol 92(1):53–62.

Salem H, Nidhal AA, Mesrati MA, Belhadj M, Quatrehomme G, Chadly A. 2014. Age estimation from the sternal end of the fourth rib: A study of the validity of İşcan's Method in Tunisian male population. Legal Med 16(6): 385-389.

Slice D, Algee-Hewitt B. 2015. Modeling bone surface morphology: a fully quantitative method for age-at-death estimation using the pubic symphysis. J Forensic Sci 60(4):835–843.

Stoyanova D, Algee-Hewitt B, Slice D. 2015. An enhanced computational method for age-at-death estimation based on the pubic symphysis using 3D laser scans and thin plate splines. Am J Phys Anthropol 136:39-50.

Stoyanova D, Algee-Hewitt B, Slice D. 2017. A computational framework for age-at-death estimation from the skeleton: Surface and outline analysis of 3d laser scans of the adult pubic symphysis. J Forensic Sci X:1-11.

Todd TW. 1920. Age changes in the pubic bone. Am J Phys Anthropol. 3(3): 285-340.

Uhl NM. 2013. Age-at-death estimation, In: Digangi EA and MK, editors. Research methods in human skeletal biology. Oxford: Elsevier. p 325-360.

Verzeletti A, Cassina M, Micheli L, Lorenzo A, and De Ferrari F. 2010. Age estimation from the rib by components method analysis in white males. Am J Forensic Med Pathol 31: 27-33.

Yavuz MF, İşcan MY, Cologlu AS. 1998. Age assessments by rib phase analysis in Turks. Forensic Sci Int. 98:47-54.